NTNU
Norwegian University of
Science and Technology

Torsion instability of Flexible Pipes at the TDP

Torsjonsinstabilitet av fleksible rør med
sjøbunnskontakt

Linn Storesund Hansson

Torsion Instability of Dynamic Flexible Risers at the Touch-Down-Point

Linn Storesund Hansson
master student at
Institute of Marin Technology,
NTNU.

Supervisor: Professor Svein Sævik
Department of Marine Structures,
NTNU.

June 9, 2017

Sammendrag (Norwegian Synopsis)

This is a presentation of the synopsis translated to Norwegian:

Stigerør er en vanlig betegnelse for fleksible rør, som er fritt eller semi-fritt opphengt mellom to punkter (offshore). Fleksible rør brukes hovedsakelig til å transportere væsker mellom plattformer/skip etc. til en strømningsledning/sjøbunnsinstallasjon eller lignende. Det sikre operasjonsvinduet for installasjonen er begrenset av vær induserte bevegelser av installasjonsfarkosten, som gir opphav til dynamiske spenninger og krumning i røret nær sjøbunnskontakt.

Ved inspeksjon og etablering av beregningsmetoder for å bestemme de faktiske grensene for installasjon og drift, ønsker denne raporten å bidra i en videreutvikle kunnskapen om global torsjonsinstabilitet av stigerør i catenary konfigurasjon ved sjøbunnskontakt. Dagens metoder er konservative, og en mulig utvidelse av drifts-/installasjonsviduet vil kunne ha direkte økonomiske fordeler for næringen.

Da tema global torsjons-stabilitet i stigerør, allerede er blitt drøftet fra før, fokuserer dette arbeidet seg på å fremme denne kunnskapen videre men med spesiell vekt på større tverrsnittdiametre. Gjennomgående analyser er gjort ved å følge allerede etablerte metoder, samt en ny metode laget for å knytte lokale effekter og feilmoduser til globale torsjonsproblemer.

Resultatene viser at ikke alle prediksjonsmetodene etablert for offshore kabler, er egnet for rør. I tillegg viser det seg at de mest kritiske bølgene, ikke alltid er de største, når det gjelder koblingen mellom dynamisk hivebevegelse og torsjons-stabilitet.

Det er funnet ut fra analysene at stigerør generelt er svært godt rustet mot global torsjonsknekking, selv når det er lokal kompresjon i røret nær sjøbunnskontakt. I tillegg, er dynamiske fleksible rør veldig motstandsdyktige mot globale torsjonsbrud under påvirkning av andre feil, som for eksempel: oversvømmelse av ringrommet og lokal lateral knekking i strekkarmeringen.

Den endelige konklusjonen er at den fremlagte oppfatningen i nyere studier rundt torsjons-stabilitet, om at dagens praksis er for konservativ, har blitt ytterligere styrket og tøyningsgrensene er mye større enn først forventet.

Synopsis

Dynamic flexible risers are a common term for cables, umbilicals and flexible pipes, that are freely or semi-freely suspended between two points (offshore). Flexible pipes are mostly used to transport fluids between platforms/ships etc. to a flow-line/sea floor installation or similar. The safe operating window for the installation is limited by weather induced motion of the installation vessel giving rise to dynamic tension and curvature at the touch-down-zone (TDZ).

By investigating and establishing calculative methods to determine the actual limits of installation and operation, this paper wishes to further the knowledge of global torsion instability of flexible dynamical pipes in catenary configuration at the Touch-down-point (TDP). Today's methods are conservative and an expansion of the operating/installation window will have direct economical benefits for the industry.

As the field of global torsion instability in flexible risers have already been touched upon before, this work centres around furthering this knowledge with special weight on larger cross-section diameter as found in flexible pipes. Thorough analysis have been made, following already established methodologies, as well as a new method made in order to linking local effects and failure modes, to global torsion problems.

The results show that not all prediction methods established for offshore cables are suitable for pipes. In addition, it is seen that when it comes to the coupling between dynamic heave motion and torsion instability, the most critical waves are not always the larger ones.

Lastly it is found from the analysis, that dynamic flexible pipes may very well resist global torsion buckling, even when there is compression at the TDP. Dynamic flexible pipes are also very good at resisting global torsion failure, while under the influence of other failures, such as flooding of the annulus and local lateral buckling of the tensile armour.

The final conclusion is that the presented opinion in newer studies on torsion instability, about the practises of today being to conservative, has been further strengthened and the limits are greater than first anticipated.

Preface

This thesis is written as the final part of the integrated master program in marine technology at the Norwegian University of Science and Technology. Proceeding this thesis is a project report concerning literature on flexible dynamic risers, and a bending analysis.

Sævik & Koloshkin (2017) presents a study of torsion instability of offshore cables/umbilicals at TDP. The study shows that the current industry practise of not allowing effective compression at TDP can be argued, as it is possible to have axial compression without kink formation given certain requirements. This has a direct economical benefit with respect to the installation cost. In addition, the paper clearly states that the load conditions leading to kink formation is fundamentally different between flexible pipes and umbilicals. This thesis is therefore furthering the work by focusing on flexible pipe configurations.

While working on this project, I have gained new insight. Not only into the mechanics of flexible pipes, but also into my own capabilities. Heading into this work, I was highly afraid of my own ability to discipline my self, and structure the extensive workload over the vast period of time. I am very thankful for my supervisor professor Svein Sævik who has helped me by dividing the project into smaller segments, and letting me take one step at a time. In addition, he has been a large influence on my motivation by always staying positive and curious. This has been a great help in the face of several computer bugs that was discovered in Bflex2010 during the process of this work.

Lastly, I would like to give a large thanks and acknowledgement to all others that have helped me in the process of making this thesis. This work would not be the same without their support.

Trondheim, June 9, 2017

Linn Storesund Hansson

Scope of Work

The report is ordered in a rational manner, first presenting: the synopsis, the preface, scope of work, applied computer programs, nomenclature and content lists. This is followed by the main body containing a presentation of theory and a literature study, before the analysis centring around Bflex2010. Each type of analysis have been separated into its own chapter to create order. The appendix contains a selection of computer input files illustrating the computational work of this thesis. Additionally, a digital copy of more input files have been submitted along with this report. Presenting the scope of work:

1. A Literature study, including flexible pipe technology, failure modes and design criteria with particular focus on the local tensile armour buckling failure mode, analytic and numerical methods for stress and tensile armour buckling analysis of flexible pipes, and the non-linear Marintek FE software Bflex2010.

2. Establishment of a realistic installation scenario including: seabed profile, water depth, route, weather data and vessel motions. On the basis of the minimum radius of curvature on the seabed, estimations of the maximum torque that can be expected during a typical installation.

3. For the two selected cross-sections, establishment of cross-section parameters in terms of: axial stiffness, torque-torsion and bending-curvature relations. This for both dry and wet annulus conditions. Also, a calculation of the minimum radius of curvature for the selected cross-sections.

4. Prediction of the critical curvature associated with kink formation for these cases and for torque.

5. Performances of dynamic analysis with built-in torque level and based on non-linear models for both torque-torsion and moment-curvature. Where the dynamic maximum curvature at TDP is used as a measurement of kink formation.

6. Use of a sufficient number of cycles in order to prove that kink formations is not developed due to accumulated plastic deformations. Where a stable value of the maximum curvature, along with obtaining a kink free formation, and at the same time the standard maximum curvature design criteria have not been exceeded, the sea state is deemed acceptable.

7. Conclusions and recommendations for further work.

Applied Computer Programs

Following computer programs were used during the work on the thesis:

Bflex2010 The thesis is based on this program. It is developed for non-linear FEM modelling and analysis of offshore pipes/cables.

Bflex2010post Bflex2010 post processing (export of the results from Bflex2010 output .raf files).

Matlab The software was used for carrying out computational operations. MATLAB scripts were also developed for reading/manipulation the data from the BFLEX2010POST output files and automatic generation of multiple plots. As well as writing (and running in batch mode) Bflex2010 input files .2bif, and writing Bflex2010post input files .2bpi, during the dynamic heave scenario.

Xpost Graphical interpretation of the results from Bflex2010 output .raf file.

Excel Used for viewing Bflex2010post output files .mpf and simple calculations, along with generating plots.

ShareLaTeX Interface for LaTeX on the cloud, that was used to write and compile the report.

Nomenclature

α Lay angle relative to the pipe longitudinal axis

β_c Curvature where slip occur

β_s curvature after slip

β_{2c} Critical slip curvature of layer

Δ Differential operator

κ Curvature

κ_t Total curvature

κ_y Curvature about the y-axis

κ_z Curvature about the z-axis

μ Friction coefficient

ν_a Apparent Poisson's ratio

ρ Bending radius

ρ_l Locking radius

ρ_s Minimum design radius

ρ_w Water density

σ Stress

σ_u Ultimate tensile strength

σ_{11} Wire normal axial stress

τ_p Overall pipe torsion

θ_0 Angle of transition between slip regions

θ_x Rotation about x-axis, torque

θ_y Rotation about y-axis

ε_p Overall pipe strain

ε_{11} Wire axial strain

A Area

$A_1/A_2/B_1/B_2$ Constants

A_t Cross-section area before slip

b Wire width

E Young's modulus

EA Axial stiffness

EI_2 Wire bending stiffness about weak axis

EI_3 Wire bending stiffness about strong axis

EI_I Initial bending stiffness

EI_s Bending stiffness after slip

F_f Fill ratio

F_x Force in x-direction

g Gravitation constant

GI Torsion stiffness

GJ Wire torsion stiffness

h Water depth

I Inertia moment

i Layer index

L Length

L_p Pitch length

M Bending moment

M_f Bending moment where slip occur

M_x Moment about x-axis, torsion moment

M_y Moment about y-axis, bending moment

n Number of wires/layers

P Axial point load/Buckling load

p Continues force

p_a End cap/axial burst pressure resistance

p_e External pressure

p_h Piston pressure

p_h Tensile armour burst pressure resistance

p_i Internal pressure

p_p Pressure spiral burst pressure resistance

p_t Nominal external pressure between pressure spiral and inner tensile armour

p_{hoop} Hoop burst pressure resistance

Q Shear force, normal to the deformed neutral-axis

q_3 Contact force per unit length

R Mean layer radius

R_h Mean helix radius

R_y Outer cross-section radius

t Thickness

T_0 Tension at TDP

T_p Total tensile loading

t_{tot} Total thickness of bout tensile armour layers

u Displacement in x-direction

u_3 Radial motion of wire

V Shear force, normal to the undeformed neutral-axis

v Displacement in y-direction

W Distributed wight

w Displacement in z-direction

x Cartesian coordinate (in longitudinal direction)

y Cartesian coordinate (in transverse direction)

z Cartesian coordinate (in height direction)

Contents

List of Figures

List of Tables

Chapter 1

Mechanics of Flexible Pipes

Dynamic flexible risers are a common term for cables, umbilicals and flexible pipes that are freely or semi-freely suspended between two points (offshore). Risers are widely used in the oil and gas industry. Flexible pipes are mostly used to transport fluids between platforms/ships etc. to a flow-line/sea floor installation or similar.

For the installation of dynamic flexible risers the J-lay method is the most applicable. The safe operating window for the installation is limited by weather induced motions of the installation vessel giving rise to dynamic tension and curvature at the touch-down-zone (TDZ).

By investigating and establishing calculative methods to determine the actual limits of installation and operation, this paper wishes to further the knowledge of global torsion instability of flexible dynamical pipes in catenary configuration at the Touch-down-point (TDP). This is in order to challenge today's conservative methods. If proven correct, expansion of the operating/installation window will have direct economical benefits for the industry.

1.1   Configuration of flexible pipes

Non-bonded flexible pipes consists of layers which are free to slide relative to each other, with only friction as a restraint (Sævik 2015). There are many different ways to layer a flexible pipe, tough certain elements will be found in most cases. Seeing from the inside there is first the steel carcass, which purpose is to help carry the external pressure and maintain the circular geometry of the pipe. Following the carcass is the inner plastic sheath, holding the transported fluid inside the pipe. Next is the pressure spiral, with a lay angel close to 90°, it carries mostly external and internal pressure. However, if there is a tear in the outer cap, it will only carry the internal pressure. The pressure spiral may consist of 1-2 layers with 1-2 wires.

Surrounding the pressure spiral is the tensile armour. Normally two helix layers

consisting of 30-80 rectangular steel wires and lay angle α in range $\pm29°$- $\pm55°$. Commonly the fraction filled ratio for the tensile armours are about 0.9 (Sævik 2015), and there are plastic anti wear layers between the steel. More precise, the fill ratio F_f can be calculated using the formula:

$$F_f = \frac{nb}{\cos\alpha 2\pi R} \tag{1.1}$$

And for pressure armour and carcass, typical fill ratio is 0.55 (Sævik 2015) and can be determined from:

$$F_f = \frac{nA}{L_p t} \tag{1.2}$$

$$L_p = \frac{2\pi R}{\tan\alpha} \tag{1.3}$$

Where n is the number of wires, b and t are the wire width and thickness, R is the mean layer radius and L_p is the pitch length.

Outside the tensile armour layers there may be a layer of anti-buckling tape, before the final outer sheath. In Figure 1.1 is an illustration of a typical dynamic flexible pipe configuration.
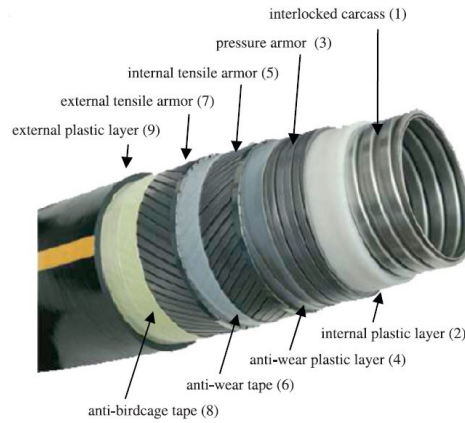
Figure 1.1: Typical flexible pipe cross-section, (Vaz & Rizzo 2011)

1.2 Small Deformations

In flexible pipes the load response is govern by the metallic layers, but the plastic layers contribute to how the load is distributed. The stress state in flexible pipes is

by nature three dimensional. However, due to the governing of structural strength by the pressure spiral and tensile armoured layers, which are composed of long slender beams, axial stress will be the primary component in strength analysis.

It is normal to assume that wires in flexible pipes rest stress free in a helix configuration, consequently secondary stress is neglected. This is due to plastic strains being introduced during manufacturing. The result is an initial torsion and initial normal curvature being different from zero. Consequently a mechanical model that takes into account the coupling between initial curvature, membrane and bending effects is needed to best describe the structural effects. According to Sævik (2015), stress in the structure is primarily induced by the following load scenarios:

- Axisymmetric loads: Changes only length and diameter of the pipe. Deformations between wires are small. Typical loads: tension, torque, internal and external pressure loads (assuming no local buckling or collapse).

- Bending loads: Results in bending of the pipeline where relative deformations between the wires will become significant.
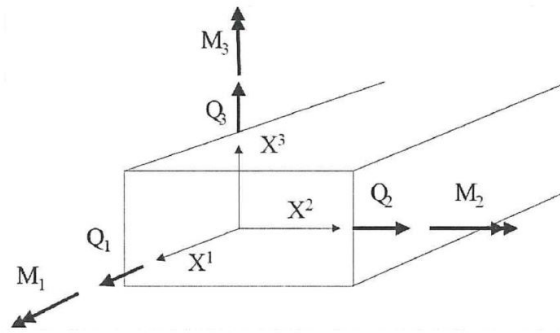
Figure 1.2: Wire stress resultants, (Sævik 2015)

Considering that the shear forces Q_2 and Q_3 are relatively small, they and the related shear stresses σ_{12} and σ_{13}, may be neglected in most cases.

1.3   Axisymmetric Loads

Using beam theory the wire equilibrium can bee described as (see Figure 1.2 & 1.3 for symbol definition):

$$-\kappa_2 Q_1 + \kappa_1 Q_2 + q_3 = 0 \tag{1.4}$$
$$-\kappa_2 M_1 + \kappa_1 M_2 + Q_2 = 0 \tag{1.5}$$

1.3.1 Tensile loads

If the armour wire is of slender geometry, the terms M_1, M_2 and Q_2 becomes small and may be neglected. Further neglecting plastic layers and only considering the steel wires, the equilibrium during pure tensile loading becomes a contribution from all the layers.
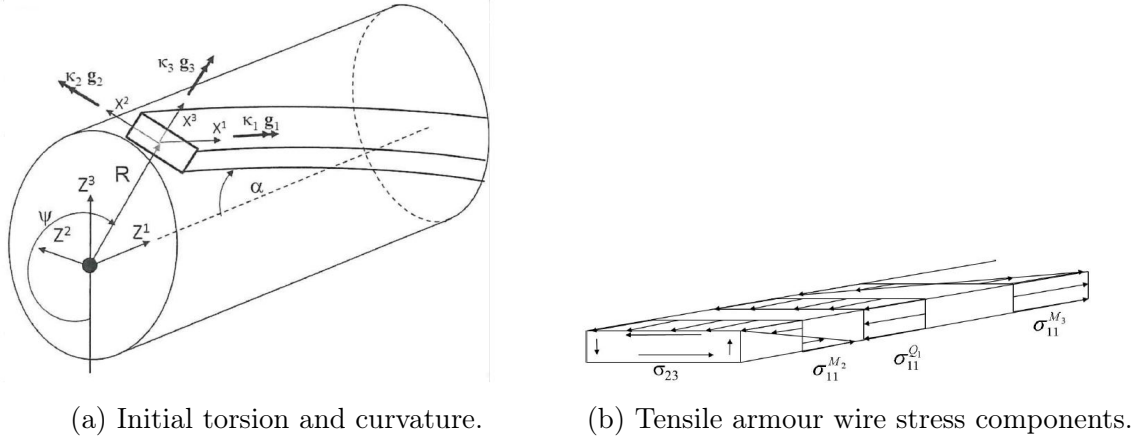
(a) Initial torsion and curvature.   (b) Tensile armour wire stress components.

Figure 1.3: Definition of wire coordinate axis and mechanical quantities.

As the lay angle α is close to zero for the carcass and pressure layer, the load is mainly taken up by the tensile armour wires. As such, one may estimate the stress in the tensile armours under the assumption that they have equal but opposite directed lay angels. Sævik (2015) gives in this case an approximation of the nominal external pressure p_t, given onto the pressure spiral by the inner tensile armour:

$$p_t = \frac{T_p \tan^2 \alpha}{2\pi R^2} \tag{1.6}$$

Where T_p is the total tensile loading. Using standard beam quantities at the cross-section centre of the pipe and the radial motion u_3, one can describe the axial strain in the helix, ε_{11}.

$$\varepsilon_{11} = \cos^2 \alpha \varepsilon_p + \frac{\sin^2 \alpha}{R} u_3 + R \sin \alpha \cos \alpha \tau_p \tag{1.7}$$

Where ε_p and τ_p are the overall pipe strain and torsion. Now, assuming that there is no torsion coupling and using energy principle, one may derive an expression for the axial stiffness, EA.

$$EA = 2\pi R t_{tot} F_f E \cos^2 \alpha (cos^2 \alpha - \nu_a \sin^2 \alpha) \tag{1.8}$$

$$\nu_a = -\frac{u_3}{R\varepsilon_p} \tag{1.9}$$

Where t_{tot} is the total thickness of both tensile armour layers, E is the elasticity-module and ν_a is the apparent Poisson's ratio. In most cases ν_a is around 0.2, making the second term in Equation 1.8 less dominating (Sævik 2015).

There will be torsion and curvature changes in the structure, though these are often small and can therefor be neglected. Nevertheless, for torsion unbalanced structures with large helical elements, these deformations have to be taken into account(Sævik 2015).

Considering torsion, in addition to tensile force, the probable damage from torsion is reduced due to the tensile force. Usually one would use the lowest axial force predicted from dynamic calculations, to set the resisters (Sævik 2015).

During production and loading, certain gaps may occur in the layers. If this happens it will have great effect on the stiffness. According to Sævik (2015), the existing methods for calculating the response from axial tension in pipes are quite reliable, but for compression the problem is more severe.

It is also important to take note of the change in α during loading. For the most part this change is small and one can set $\alpha = \alpha_0$. However, at the end of the pipe, if the lay angle is restricted form changing, this will cause local bending stresses. These stresses are very important for fatigue and life time calculations (Sævik 2015).

1.3.2 Pressure loads

If a pipe is experiencing internal pressure, the approximate equilibrium equation may be put up as follows (Sævik 2015):

$$\sum_{j=1}^{N_a} \frac{\eta_j \sigma_{11j} A_j \sin^2 \alpha_j}{R_j} \frac{1}{\cos \alpha_j} = 2\pi(p_i R_i - p_e R_e) \tag{1.10}$$

Where N_a is the number of pressure resisting layers, σ_{11} is wire axial stress, p_i is internal pressure, p_e is external pressure. Here it is assumed that the plastic layers simply transfer stress and that the interlocked carcass does not carry any load. This equation in combination with Equation 1.1 gives the tensile armours resistance contribution to the burst pressure, p_h.

$$p_h = \frac{t_{tot}}{R} F_f \sigma_u \sin^2 \alpha \tag{1.11}$$

Where σ_u is the ultimate strength of the tensile armour layers. Further, Sævik (2015) provides the following simplifications for the end cap burst pressure resistance p_a, and the resistance from the pressure spirals p_p:

$$p_a = 2\frac{R}{R_{int}^2}t_{tot}F_f\sigma_u \cos^2\alpha \tag{1.12}$$

$$p_p = \sum_{j=1}^{N_p} \frac{t_j}{R}F_{fj}\sigma uj \tag{1.13}$$

Summing up the resistance form each layer the hoop resistance becomes:

$$p_{hoop} = p_p + p_h \tag{1.14}$$

Then the burst pressure will be given by the minimum of the hoop pressure resistance and the axial resistance.

1.4 Bending of Pipes

1.4.1 Slip Moment

For small curvatures, slip between the layers is prevented by friction. This gives a rather high initial bending stiffness EI_s. To overcome the friction forces, a moment M_f, denoted friction moment, is needed. As the bending moment exceeds M_f, it will vary linearly in relation to the bending curvature, though with the stiffness EI_e. This stiffness is quite small compared to the initial stiffness, as the main part comes from the plastic layers. For reverse loading, the change in curvature should be larger than $2M_f$ for slip to reoccur (Sævik 2015).

Considering the tensile armour, the stresses will be given by the mean static tension and related pressures. These reactions will effect the friction moment M_f. As the tension and external pressure may vary along the length of the pipe, so will the friction moment. In addition, as the contact pressure between layers differs, the dynamic behaviour of pipe stresses will be characterized by change in both longitudinal and radial direction.(Sævik 2015)

At the beginning of bending, the pipe will behave rigidly. Though, as the bending continues the shear stress will exceed the limit of resting friction, introducing slip. According to standard beam theory, the maximum shear will occur at the neutral axis. The shear stress will increase with bending, until the maximum capacity q_{1c} is reached. (Sævik 2015) sets the corresponding critical curvature to be:

$$\beta_{2c} = \frac{\mu(q_3^i + q_3^{i+1})}{\sin\alpha A_t} \tag{1.15}$$

Where μ is the friction coefficient, q_3 is the contact force per unit length, A_t is cross-section area before slip, and the index i denotes the inner and outer surface of the considered armour wire.
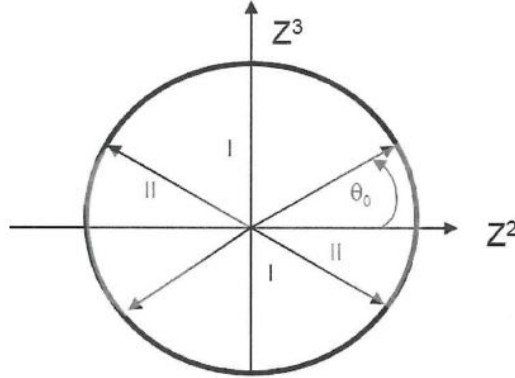
Figure 1.4: Cross section stick and slip regions, (Sævik 2015).

If one assumes no end effects and harmonic helix motion, an arbitrary cross-sections may be divided in two regions, as seen in Figure 1.4 One being the stick region (Region I) and the other the slip region (Region II). In relation to Figure 1.4, one can see that the transition between these two regions will be at the angle θ_0 (Sævik 2015).

$$\frac{\theta_0}{\sin \theta_0} = \frac{\beta_s}{\beta_{2c}} \tag{1.16}$$

where β_s is the curvature at any point beyond full slip. Considering the armour layer as a thin shell structure with thickness t, (Sævik 2015) proposes this description of the bending moment:

$$\begin{aligned}
M = 4F_f \cos 2\alpha [&\int_0^{\theta_0} \frac{\mu(q_3^i + q_3^{i+1})}{\sin \alpha A_t} \theta \\
+ &\int_{\theta_0}^{\frac{\pi}{2}} E \cos^2 \alpha \beta_2 (\sin \theta - \sin \theta_0) + \frac{\mu(q_3^i + q_3^{i+1})}{\sin \alpha A_t} \theta_0] t R^3 \sin \theta d\theta
\end{aligned} \tag{1.17}$$

Using equation 1.15 and 1.17 a moment curvature diagram can be put up as seen in Figure 1.5.

Aforementioned, the contact pressure varies between layers, following this the moment-curvature diagram for the whole pipe will be a sum of the contribution from each layer. Nevertheless, as the transaction in curvature between start of slip and full slip is small, the diagram of the total effect may be approximated using bi-linear relations.

Assuming that the plane surfaces do not remain plane during bending, which would be the case for pipes with thick plastic layers, the equation 1.15 no longer holds. For this case (Sævik 2015) presents the following equation:
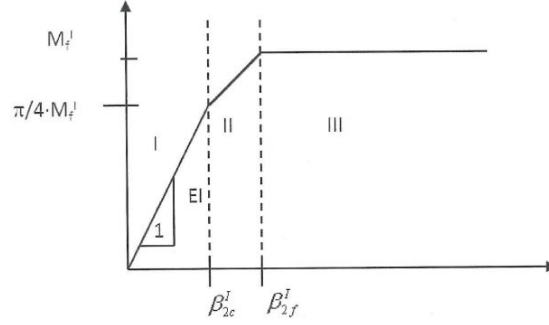
Figure 1.5: Moment curvature diagram, (Sævik 2015).

$$\beta_{2c} = [1 + \frac{\sin^2 \alpha EA_t}{kR^2}]\frac{\mu(q_3^i + q_e^{i+1})}{EA\cos^2\alpha\sin\alpha} \tag{1.18}$$

From the previous equation it is reasonable to assume that the introduction of the shear stiffness parameter k, will enlarge the critical slip curvature. As a result, the stress in the stick domain will decrease. According to (Sævik 2015) a shear interaction model is better at describing the transaction than a model using plane surface approximation. However, for fatigue analysis the value k becomes critical for the result, and a number of model tests is needed in order to give high enough confidence level.

1.4.2   Locking Radius

For excessive bending, interlocking between elements can occur, or the elements in the helical armours starts to interfere by touching each other. In addition, the plastic layer may be over strained. The limit at which either of these occur, is described as the locking radius ρ_l. As each steel layer in the pipe will have its own locking radius, the largest one is considered. (Sævik 2015)

According to *API17J* the smallest allowed design radius ρ_s for dynamical cases is given as:
$$\rho_s = \rho_l * 1.1 * 1.5 \tag{1.19}$$

For a dynamic riser in catenary configuration the required bottom tension T_0 is then given by (Irgens 2014):
$$T_0 = \rho_s * W \tag{1.20}$$

where W is the distributed weight of the riser (including buoyancy).

1.5 Buckling

1.5.1 Greenhill

Buckling is an instability problem often referred to as: "the second order problem" (Bažant & Cedolin 1991). This is due to the form of the equilibrium equation for a deflected beam-column, given by:

$$(EIw'')'' + (Pw')' = p \tag{1.21}$$
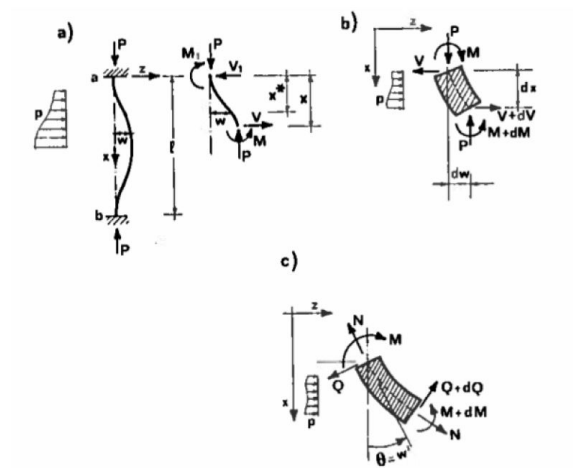
Figure 1.6: Equilibrium of (a) a segment of a statically indeterminate column and (b, c) of an infinitesimal element (Bažant & Cedolin 1991).

Where EI is the stiffness, w is displacement, and p and P are loads with reference to Figure 1.6. The equation may be derived in the following way; considering a segment of a deformed column (see Figure 1.6), with a continuous horizontal load p and a vertical point load P. The equilibrium of the segment is

$$V(x) - V_1 + \int_0^x p(x^*)dx^* = 0 \tag{1.22}$$

$$M(x) + Pw(x) - M_1Vx \int_0^x p(x^*)x^*dx^* = 0 \tag{1.23}$$

Where M is the moment and V is the shear force. By differing the Equations 1.22 & 1.23 and substituting in order to simplify, one gets:

$$V' = -p \quad \text{and} \quad M' + Pw' = -V \tag{1.24}$$

Then the second of Equation 1.24 is differentiated once more, and the first equation is substituted to get:

$$M'' + (Pw')' = p \tag{1.25}$$

Now using the relation $M = EIw''$, which is known from classical bending theory, one is back at the first equilibrium Equation 1.21.

A variant of the beam-column problem is the pressurised pipe. Assume a pipe filed with water and pressurised by a piston, as shown in Figure 1.7. Considering an infinitesimal along the length of the pip, the equilibrium of the horizontal forces and the moment around the centroid of the pip gives us:

$$V' = 0 \quad \text{and} \quad M' + p_h Aw' = -V \tag{1.26}$$

Where p_h is piston pressure and A is piston area. Doing the same as was done to get Equation 1.24 from Equation 1.21, previously. The relation $M = EIw''$ is used, and one gets:

$$(EIw'')'' + (p_h Aw')' = 0 \tag{1.27}$$

In order to consider torque, the equilibrium Equation 1.21 must be generalised. Also, the contribution from the torque must be added. Assuming that EI is the same in z and y direction (as it in a symmetrical pipe) this gives us the new differential equations:

$$(EIw'')'' - M_x v' + (Pw')' = 0 \tag{1.28}$$
$$(EIv'')'' - M_x w' + (Pv')' = 0 \tag{1.29}$$

which will have a general solution on the form:

$$v = Ae^{iwx} \quad w = Be^{iwx} \tag{1.30}$$

By substituting Equation 1.30 in to Equations 1.28 & 1.29, one may simplify to get the following homogeneous linear equation:

$$\begin{bmatrix} P - EIw^2 & iM_x w \\ -iM_x w & P - EIw^2 \end{bmatrix} \left\{ \begin{array}{c} A \\ -iM_x w \end{array} \right\} = \mathbf{0} \tag{1.31}$$

One may only have deflection if the determinant equals zero. Considering torque of only one sign, it gives the roots:
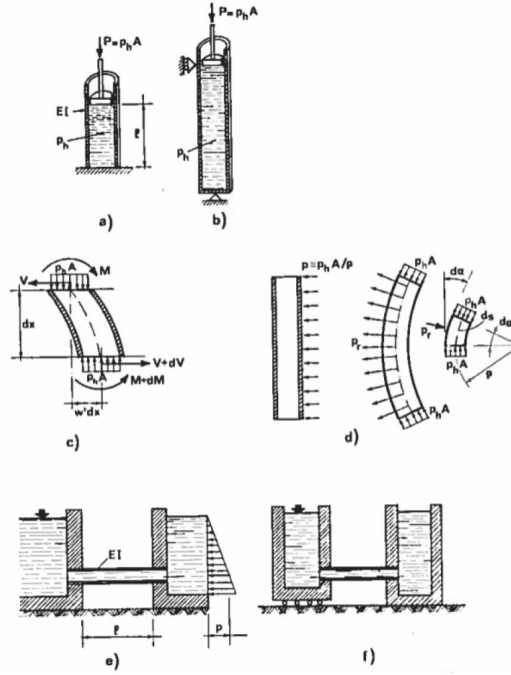
Figure 1.7: Buckling of hydraulic column supports and pressurised pipes (Bažant & Cedolin 1991).

$$w_{1,2} = \frac{1}{2EI}\left(- M_x \pm \sqrt{M_x^2 + 4EIP}\right) \tag{1.32}$$

As such the general solution will be the real or imaginary part of:

$$v = A_1 e^{iw_1 x} + A_2 e^{iw_2 x} \quad w = B_1 e^{iw_1 x} + B_2 e^{iw_2 x} \tag{1.33}$$

With the complex constants A_1, A_2, B_1 and B_2. For a hinged beam the boundary conditions are $w = v = 0 \vee (x = 0 \cup x = l)$. This gives the following conditions:

$$A_1 + A_2 = 0 \qquad A_1 e^{iw_1 l} + A_2 e^{iw_2 l} = 0 \tag{1.34}$$

$$B_1 + B_2 = 0 \qquad B_1 e^{iw_1 l} + B_2 e^{iw_2 l} = 0 \tag{1.35}$$

Lets now assume that $B_1 = B_2$, there will only be a nontrivial solution if $e^{iw_2 l} = e^{iw_1 l} \Rightarrow w_1 l = w_2 l + 2\pi n$. In the first critical case $n = 1$, which gives $w_2 = w_1 + \frac{2\pi}{l}$. Looking at Equation 1.32, this yields $\frac{(M_t^2 + 4EIP)^{0.5}}{2EI} = \frac{\pi}{l}$. One may then write this equation as:

$$\frac{P}{P_{cr}^0} + \left(\frac{M_x}{M_{cr}^0}\right)^2 = 1 \tag{1.36}$$

where

$$P_{cr}^0 = \frac{\pi^2}{l^2}EI \quad M_{cr}^0 = k\frac{\pi EI}{l} \quad k = 2 \tag{1.37}$$

Equation 1.36 is known as the Greenhill equation and was established in 1883, by the person of the same name (Bažant & Cedolin 1991).

1.5.2 Local Buckling

From the extended use of flexible pipes, there have been, over the two last decades, experienced and identified numerous failure modes for flexible pipes. As pipelines are usually installed empty, there is no internal pressure to balance the external pressure. For deep water installation, this will lead to significant compression stresses in the tensile armour and local buckling may occur (Sævik 2015).

Collapse of the Carcass

If the pipe is exposed to excessive external pressure collapse may occur, e.g., at deep water depths. This usually involves ovalization of the pipe, and thus obstruct the internal fluid flow. As design depths are commonly well defined, this is often not seen as a critical failure mode.

In order to verify the design depth, one must use atmospheric internal pressure as this will be the most critical state. Assuming that there is a tear in the outer sheet, the pressure wire will not carry external loads and the carcass will be the only effective carrier. Producers therefore mostly only use the strength of carcass when determining collapse pressure (Sævik 2015).

To find the collapse pressure of the carcass Sævik (2015) proposes the Timoshenko method from "Theory of Elastic Stability" by Timoshenko and Gere (1969). The theory bases itself on the assumption of an initial imperfection, and then considers the bending moment. The elastic buckling pressure of the carcass can be found as a sum of the contributions from the carcass and the pressure spiral layer. This is valid under the assumption of there being no gaps between the pressure armour layer (Sævik 2015). However, if there is gaps, the effect from the surrounding layers on the carcass will lessen, and the pressure capacity will reduce dramatically. Furthermore, addition of other external forces will contribute to increased ovalization and therefore increase the reduction of the capacity.

Buckling in the Tensile Armour

Under installation and also during shut down condition, there is no internal pressure. The external overpressure will then introduce local compression in the tensile armour, even though the overall tension of the pipe can be positive. The compression may

cause local buckling in the tensile armour wires, leading to global torsion instability of the pipe.

Vaz & Rizzo (2011) presents a FEM-study on the influence of friction, interlaying contact behaviour and the anti-buckling tape capacity during pure external pressure. The study identifies four different failure modes, depending on friction and the anti-buckling tape capacity. Two failure modes are related to lateral instability and the other two related to radial instability (Bird-caging).

In the lateral instability modes the anti-buckling tape is intact, while the radial instability modes seems to be related to the failure of the anti-buckling tape and elastic foundation buckling. The paper concludes that the most critical condition is experienced when the annular is flooded. This is despite the fact that the external compressive pressure is reduced. In this case the anti-buckling tape must carry the radial expansion load from the tensile armour alone and therefor also determine the critical pressure (Sævik 2015).

The determination of the critical pressure must be done in combination with different triggering modes. A study of different triggering modes of the birdcaging phenomena was done by Rabelo, Pesce, Santos, Ramos, Franzini & Gay Neto (2015).
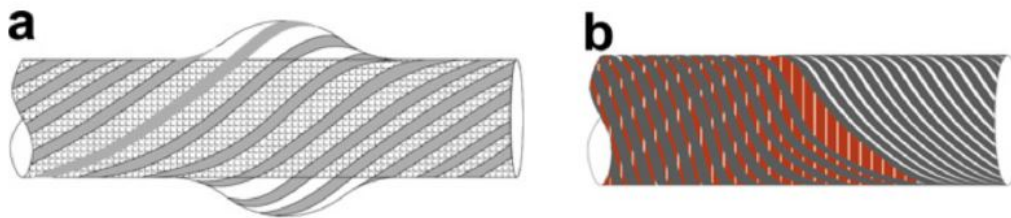
Figure 1.8: Local buckling mods: (a) Bird-caging, (b) Lateral buckling. (Vaz & Rizzo 2011)

Considering lateral buckling, this is a failure mode that happens while the antibuckling tape is intact. As the wire may not go outwards, it is forced to go sideways. The friction forces are smallest for the inner layer, and it will therefor lose its axial force capacity first. Consequently, the outer layer have to lessen the uptake of axial force to keep the torsion balance of the pipe. This will result in a rotation of the pipe in the direction of the lay angel of outer tensile wires.

In case of cyclic loading, e.g., heave motion of production vessel, there will be induced a small plastic rotation per cycle, evidently resulting in torsion failure of the cross-section (Sævik 2015). The danger with lateral buckling is that in contrast to radial buckling, it is hard to visually detect, and it may therefore continue to propagate undiscovered.

In order to determine local wire buckling, a finite element methodology and analytic models were presented by Sævik & Thorsen (2012). In addition, one may use the formula in Equation 1.38, which is a conservative estimate of the transverse buckling load, assuming no friction between layers (Sævik & Ji 2014).

$$P = \frac{n \cos \alpha}{R_h^2}[GJ \sin^4 \alpha + (4EI_2 + EI_3 - GJ) \sin^2 \alpha \cos^2 \alpha] \qquad (1.38)$$

Where n is the number of wires, α is the helix lay angel relative to the pipes longitudinal axis, R_h is the mean helix radius, GJ is the wire torsion stiffness, EI_2 is the wire bending stiffness about weak axis and EI_3 is the wire bending stiffness about strong axis.

1.5.3 Global Buckling

Pipelines resting on the seabed

If a pipeline is exposed to increase in internal pressure and/or increase in temperature it will try to expand. Due to contact friction with the soil the expansion will be restrained, resulting in an external compression force along the pipe. This force may introduce buckling, either vertical (upheaval buckling) or a combination of vertical and horizontal (snaking).

Figure 1.9: Lateral snaking

Upheaval buckling is most common for buried lines as the horizontal degrees of freedom are restrained by the surrounding soil. For pipelines exposed on the seabed, bending will start as upheaval buckling and at a certain height, horizontal buckling will take place. As flexible pipes have soft bending stiffness, they are weaker against bucking loads and triggering. Therefore, flexible pipes are most often buried to protect the mechanical properties. (Sævik 2015)

Risers in Catenary Configuration

During the installation process the riser will end up hanging almost vertically down from the installation vessel. This in combination with low tension at the area close to the seabed, the touchdown zone (TDZ), lowers the risers resistance towards torsion instability.

With the addition of torsion moment, possibly either from manufacturing imbalance of the armour layers or yaw movement of the installation vessel etc., a looping condition known as "hocking" may occur. Further, if the tension is increased after looping one risks the formation of a kink, resulting in failure of the riser.

It is up to discussion whether torsion instability of a riser is of static or dynamic nature. Looking at some of the significant loads the riser is subjected to, there is a combination of conservative and non-conservative static loads. Examples of this are the weight of the riser, along with internal and external pressure, and contact with the seabed. These loads are then in combination with highly dynamic loads, like: vortex induced vibrations (VIV), inducing currents, wave loads and motions of the installation vessel.

VIV are hard to calculate and should be determined using close to real scenario experiments for individual cases, due to high dependence on Reynolds number. Therefore the problem of current loads is often simplified for slender structures by taking drag forces into account by using Morison's formula.

Neto & de Arruda Martins (2013) presents a methodology to calculate tension instability issues of risers in catenary configuration. The methodology is backed up by a case-study of different types of riser environments, though it seems to mainly focus on umbilicals and cables. The case-study also assumes that the riser will behave as a rigid structure, not taking slip between layers into account, after the base catenary configuration is set.
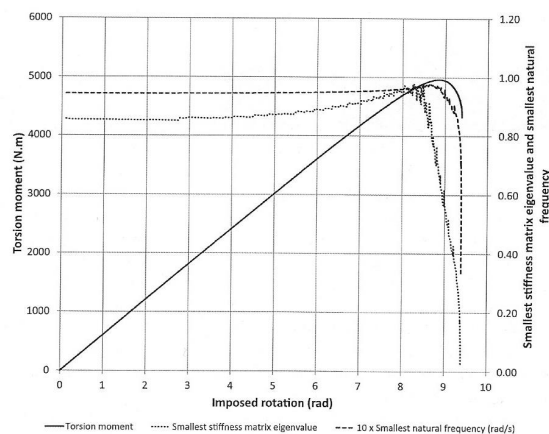
Figure 1.10: Results for riser in catenary configuration, with 89.6 °top declination angle and seabed friction $\mu = 0.4$, (Neto & de Arruda Martins 2013).

The study (Neto & de Arruda Martins 2013) shows that the calculated result of riser behaviour at the TDZ is dependant on the modelling of the seabed contact. The most realistic model in the paper, is when the pipe is allowed to slide along the seabed constrained only at the very end and by contact friction. A result from this type of model is presented in Figure 1.10, showing the smallest stiffness matrix Eigenvalue

over imposed rotation. Note that the Eigenvalue drops to zero close to the instability limit of the riser. The drop is relatively steep and fine steps are needed to catch it.

Another discovery by Neto & de Arruda Martins (2013) is that the geometrical behaviour of the riser will change dependent on the seabed friction. For friction free cases the riser simply lifts up at the TDP when the loop is formed, not touching the seabed again at this point. On the other hand, when there is friction the riser bounces on the seabed surface during looping to avoid the lateral displacement restriction given by the friction.

1.6   Fatigue

For flexible risers the most critical place with respect to fatigue is the top connection point to the platform, the touch down point, and the sagging and hogging sections (Sævik 2015). The calculation of fatigue life of dynamic flexible risers is often done in a three step process:

1. Determination of annual fatigue load given by tension and curvature/angles over a time series, from global analysis.

2. Local analysis to find stresses related to the global analysis.

3. Sorting the stress from local analysis into stress ranges to be used in a Miner sum to calculate the fatigue damage.

The governing layer of metal fatigue life is most often the tensile armour. The armour's composition of cold formed steel gives it a high yield stress, but also makes it sensitive to corrosion. Due to the risk of tears in the outer sheet, corrosion effects from seawater needs to be taken into account. Also, depending on the transported fluid, there can be leakages of H_2S and/or CO_2, resulting in brittling of the metal. Another aspect is that fatigue depends on the friction between the anti-wear layers.

These layers' performance are strongly tied to operating temperature, manufacturing and thickness. Considering that some of the tensile wires may fail, there are a number of consequences, Sævik (2015) lists these:

- Reduction of the axial force capacity, resulting in axial elongation given true wall tension.

- Rotation in direction of failed layer to ensure torsion balance (see bottom of sub-section: 1.5.2, Buckling in the tensile armour).

- Lastly, there will be an increase of mean and dynamic stress in the tensile armour, and also in the pressure spiral.

It is hard to determine how many failures there can be allowed, as the placing of the failures relative to each other play a key part. The important question is whether there is a possibility to detect the torsion rotation before global failure occurs.

Chapter 2

Analysis

2.1 Bflex2010

This section will give a short presentation of the theories applied in BFLEX2010 given by the BFLEX2010 - Theory Manual (Sævik 2013) and BFLEX2010 - User Manual (MARINTEK BEFLEX Dev. Team 2016). BFLEX2010 is a computer program for non-linear static and dynamic analysis of flexible pipes, using FEM. The program is developed as a joint industry project by MARINTEK (Now: Sintef Ocean) and Department of Structural Engineering. From its diversity of special made elements, BFLEX2010 is capable of solving most flexible pipe related problems, and provides a useful tool for stress and fatigue analysis.

2.1.1 Principle of Virtual Work

This principle states that the internal work of the structure should equal the external work for an arbitrary virtual displacement. This is approximately given by a sum of weighted functions, and so one obtains a type of integrated equilibrium when the boundary conditions are met. However, even if there is an overall equilibrium, this may not hold true for an arbitrary point within the volume.

Not taking into account volume forces, the formula for virtual work for a body in an arbitrary equilibrium with deformed volume V and surface S, is given as:

$$\int_V (\rho \ddot{\mathbf{u}} - \mathbf{f}) \cdot \delta \mathbf{u} \ dV + \int_V \boldsymbol{\sigma} : \delta \boldsymbol{\varepsilon} \ dV - \int_S \mathbf{t} \cdot \delta \mathbf{u} \ dS = 0 \qquad (2.1)$$

Where the material density is given as ρ, the acceleration field is $\ddot{\mathbf{u}}$, the volume force vector is $\mathbf{f}$, the displacement vector is $\mathbf{u}$, $\boldsymbol{\sigma}$ is the Cauchy stress tensor, with $\boldsymbol{\varepsilon}$ as the natural strain tensor, and $\mathbf{t}$ is the surface traction.

As the program handles non-linearities such as large deformations an incremental form of the principle virtual work is needed. BFLEX2010 uses the Co-rotational Total

Lagrangien formulation. Utilising the equation (2.1) for an increment Δ, including static terms only, the formulation yields:

$$\int_V \mathbf{C} : (\boldsymbol{\varepsilon} + \boldsymbol{\Delta}\mathbf{E}) : \delta(\boldsymbol{\varepsilon} + \boldsymbol{\Delta}\mathbf{E}) \, dV_0 - \int_S (\mathbf{t} + \boldsymbol{\Delta}\mathbf{t}) \cdot \delta\mathbf{u} \, dS_0 = 0 \qquad (2.2)$$

Where $\mathbf{E}$ is the Green strain tensor. The (2.1) equation gives the basis for BFLEX2010's formulation of the stiffness matrix, where the first term provides the material stiffness, and the second term gives the geometric or initial stress stiffness matrix.

2.1.2   Pipe52

The pipe element Pipe52 have been used for the prestudy analysis. This is an elastic/elastoplastic element that may be used to handle the core and resultant moment based model for the armour layers. The wire kinematics and stress-strain relations of the element follows three main assumptions:

1. Considering only doubly symmetric cross-sections.

2. Neglecting insignificant second order terms in the Green strain tensor.

3. Euler-Bernoulli beam assumption of no shear deformations along the long and slender rod.

Where the governing stress-strain components are given by Hooke's law.

The element uses two types of models to represent the behaviour. The first is the axisymmetric model which is based on the following assumptions:

1. Regularity of initial geometry:

   - The structure is strait.

   - Homogeneous layers are long and uniform.

   - The wires are wounded in a perfect helix, with equal spacing.

   - The force from the armours on neighbouring layers can be described by uniform pressure.

2. Reduction to simple plane analysis:

   - Field loads (such as self-weight), and end effects are neglected.

   - The longitudinal displacement and twist of a material point is the same for all layers.

   - An armour layer's wires all presents the same stress state and maintain a helical configuration when strained.

   - The angle between the wire cross-section principal inertia axis and a radial vector, going from the structure's cross-section center to the center of the wires cross-section, is constant.

- There is no gap spanning or over-penetration.

3. Linearity of the response:

  - Linear elastic behavior of the materials.

  - The changes in armour radii and pitch angel are small.

  - There is no void between layers.

  - The homogeneous layers simply transfer pressure.

  - The core of the pipe responds linearly to axisymmetric loading.

  - Loading and response are not time dependent.

The second type of models are the bending models. During bending, the pipe will first behave like a rigid pipe according to Navier's hypothesis. At a certain point however, slip will occur. The slip model uses the assumption of plane deformation only, which yields that the needed shear force per unit length along the wire q_1, in the tendon is:

$$q_1 = EA \cos^2 \alpha \sin \alpha \sin \psi \beta_2 \tag{2.3}$$

Where E is the Young's modulus, A is the wire cross-sectional area, α is the lay angel relative to the pipe longitudinal axis, while ψ and β_2 is represented in Figure 2.1. The shear force is increased until it reaches its critical value q_{1c}.

$$q_{1c} = \mu(q_3^I + q_3^{I+1}) \tag{2.4}$$

Where μ is the friction coefficient and q_3 is the line contact load for layer I.
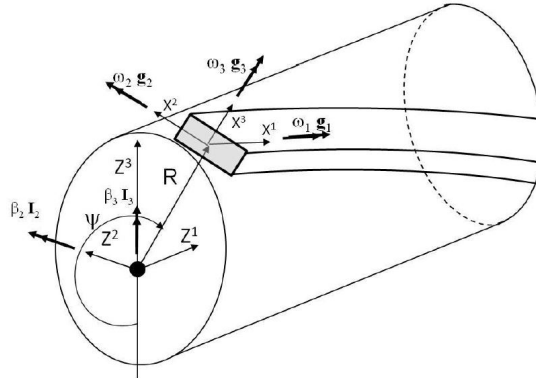

Figure 2.1: Kinematic Quantities and Coordinate System Definition, (Sævik 2013).

The Pipe52 element then uses a Moment-curvature model to establish an incremental constitutive relation.

$$
\begin{bmatrix} \Delta M_{Z^2} \\ \Delta M_{Z^3} \end{bmatrix} = EI \begin{bmatrix} 1 - \frac{M_2^2}{M^2(1+\Phi/EI)} & -\frac{M_2 M_3}{M^2(1+\Phi/EI)} \\ -\frac{M_2 M_3}{M^2(1+\Phi/EI)} & 1 - \frac{M_3^2}{M^2(1+\Phi/EI)} \end{bmatrix} \begin{bmatrix} \Delta \beta_2 \\ \Delta \beta_3 \end{bmatrix} \tag{2.5}
$$

2.1.3 Pipe31

Pipe31 is a simple linear elastic 2-noded beam element, applying plane stress assumption and Hook's law. The element is simplified by utilising that the hoop stress is known by using thin shell theory.

2.1.4 Compipe42

Compipe42 uses a resultant based material model and may describe the material behaviour either by using a HYCURVE model or a EPCURVE model. The main Principal of the HYCURVE model is a non-linear material resultant quantity expressed as a one to one function of the associated deformation quantities, with no hysteresis. In the analysis presented in this paper the HYCURVE is used to express the force-strain relation in longitudinal direction $F_x \Leftrightarrow \varepsilon_x$, and the torsional moment-rotation relation $M_x \Leftrightarrow \frac{\theta_x}{L}$.

The EPCURVE model is an elastoplastic material model and enables hysteresis. By choosing the hardening parameter ϕ, the hardening may be either isotropic $\phi = 0$ or kinematic $\phi = 1$. This model, given kinematic hardening, was used to describe the bending moment-curvature relation for the following analysis using the Compipe42 type element.

Figure 2.2: Kinematic and Isotropic Hardening, (Sævik 2013).

2.1.5 Cont126

Cont126 is a 1-noded 3D seabed contact element, which is linked to the contact surface definition. The element uses resultant based material models as described in Subsection 2.1.4. In addition, it allows for different material behavior for different

penetration depths. In this paper however, only one material behaviour for the soil is given.

2.1.6 Sea150

In, BFLEX2010, all physical effects are forced into the concept of elements and nodes. The Sea150 element simulates the sea properties and is represented by an arbitrary number of 4-noded shell elements. By defining a contact interference between the sea element and the structural element groups, buoyancy force effects are applied. In addition, using the WAVE commando, drag effects and wave forces will be included.

2.1.7 Hshear363

Hshear363 is a 3-noded 15 DOF beam-shell element. Firstly there are the to standard beam end nods with 6 DOFs each, which handles axial strain and torsion. In addition there is an extra 3 DOF centre node to take care of circumferential strain and ovalization. The purpose of the element is to more accurately handle plastic layers, the pressure armour layers and tape layers.

For the helix layers, the resulting longitudinal strain is:

$$\epsilon_{11} = \cos^2 \alpha w_{1,1} + \frac{\sin^2 \alpha}{R} u_3 + R \sin \alpha \cos \alpha \chi_{1,1} - u_{3,22} \sin^2 \alpha X^3 \qquad (2.6)$$

While for the plastic layer the strain quantities are:

$$\varepsilon_{11} = w_{1,1} + w_{3,11} R \cos \psi - w_{2,11} R \sin \psi \qquad (2.7)$$

$$\varepsilon_{22} = \frac{u_3}{R} - u_{3,22} X^3 \qquad (2.8)$$

$$\varepsilon_{12} = R \chi_{1,1} \qquad (2.9)$$

$$(2.10)$$

2.2 Geometries

In this paper two different pipe geometries (see Table 2.1) have been analysed. The pipes have been tested for wet state, meaning that there is a tear/leak in the outer cap resulting in a flooded annulus, and dry state where the outer cap i whole.

Table 2.1: Geometries used in the analysis

Type of pipe		6"	14"
Carcass	Thickness [mm]	6	7.2
Inner pressure barrier	Thickness [mm]	5.3	21
Pressure spiral	Thickness [mm]	9	10
	Wire area [mm^2]	114.8	127.5
	Lay angle [deg]	88.5	89.4
	Pitch-Length [mm]	15	15
	Wire width [mm]	19	20
Anti wear layer	Thickness [mm]	1	1
Inner tensile armour	Thickness [mm]	3	4
	Wire width [mm]	10	15
	Number of wires	52	70
	Wire area [mm^2]	30	60
	Lay angle [deg]	26.2	31.5
Anti wear layer	Thickness [mm]	1	1
Outer tensile armour	Thickness [mm]	3	4
	Wire width [mm]	10	15
	Number of wires	54	72
	Wire area [mm^2]	30	60
	Lay angle [deg]	-26.2	-31
Bird caging tape	Thickness per layer [mm]	1	1
	Layers	1	2
	Width [mm]	60	60
	Lay angle [deg]	83.5	-84.5
Outer sheath	Thickness [mm]	6	10

Chapter 3

Prestudy

3.1 Method Prestudy

To determine the global material behaviour of the pipes, small sections of 10 cm were analysed using Pipe52 elements. All the sections were exposed to an external pressure equivalent of 2000 m water depth during the tests.

Considering the material properties used in the prestudy, the steel was assigned an elasticity modulus of 210 GPa, while the tape and plastic parts have been given an elasticity modulus of 0.4 GPa. The Poison's ratio was set to 0.3 for the steel, and for the tape and plastic to 0.4.

First the sections were clamped at one end and then elongated in longitudinal direction using a prescribed displacement u, to determine the axial stiffness EA. Which is given by the formula:

$$EA = \frac{\Delta F_x}{\Delta u} \tag{3.1}$$

where F_x is the total axial force, given by the sum of the contribution from each layer.

Secondly, the sections were given a prescribed rotation about the x-axis θ_x, to determine the torsion stiffness GI. Given by:

$$GI = \frac{\Delta M_x}{\Delta \theta_x} L \tag{3.2}$$

where M_x is the total torsion moment and L is the length of the section.

Thirdly, a bending analysis was preformed by imposing a prescribed rotation about the y-axis θ_y, in both ends. From the bending analysis one can determine the slip moment M_f and corresponding curvature β, as well as the initial bending stiffness EI_I and the slip stiffness EI_s. The bending stiffness may be found from the correlation:

$$EI = \frac{\Delta M_y}{\Delta \kappa} \tag{3.3}$$

$$\kappa = \frac{1}{\rho} = \frac{2\theta_y}{L} \qquad (3.4)$$

where M_y is the total bending moment, κ is the curvature and ρ is the bending radius.

During the bending analysis the 6" pipe is considered to have a tensile loading of 50 kN and the 14" pipe has a tensile loading of 70 kN. The pipes are modelled for installation state, which equals zero internal pressure. Though, to ensure stability during calculation, a small internal pressure of 0.7 bar was added to the models.

3.2 Result Prestudy

The result of axial, torsional and bending stiffness for the different pipe geometries and states is presented in Table 3.1.

Table 3.1: Pipe stiffness

	6" Dry	6" Wet	14" Dry	14" Wet
EA $[N]$	$6.33 * 10^8$	$6.33 * 10^8$	$1.13 * 10^9$	$1.12 * 10^9$
GI $[Nm^2]$	$1.59 * 10^6$	$1.59 * 10^6$	$2.09 * 10^7$	$2.07 * 10^7$
EI_I $[Nm^2]$	$2.70 * 10^6$	$2.70 * 10^6$	$2.26 * 10^7$	$2.25 * 10^7$
EI_s $[Nm^2]$	$1.27 * 10^5$	$1.99 * 10^4$	$1.31 * 10^6$	$4.21 * 10^5$

One sees that EA, GI and EI_I is about the same for pipes with the same geometry, while EI_s differs depending on the state. Looking at Figure 3.1, there is significant change in the slip moment and curvature between states. The low values in wet state is due to reduction in friction force because of flooding of the annulus.

(a) 6" pipe in dry state.

(b) 6" pipe in wet state.

(c) 14" pipe in dry state.

(d) 14" pipe in wet state.
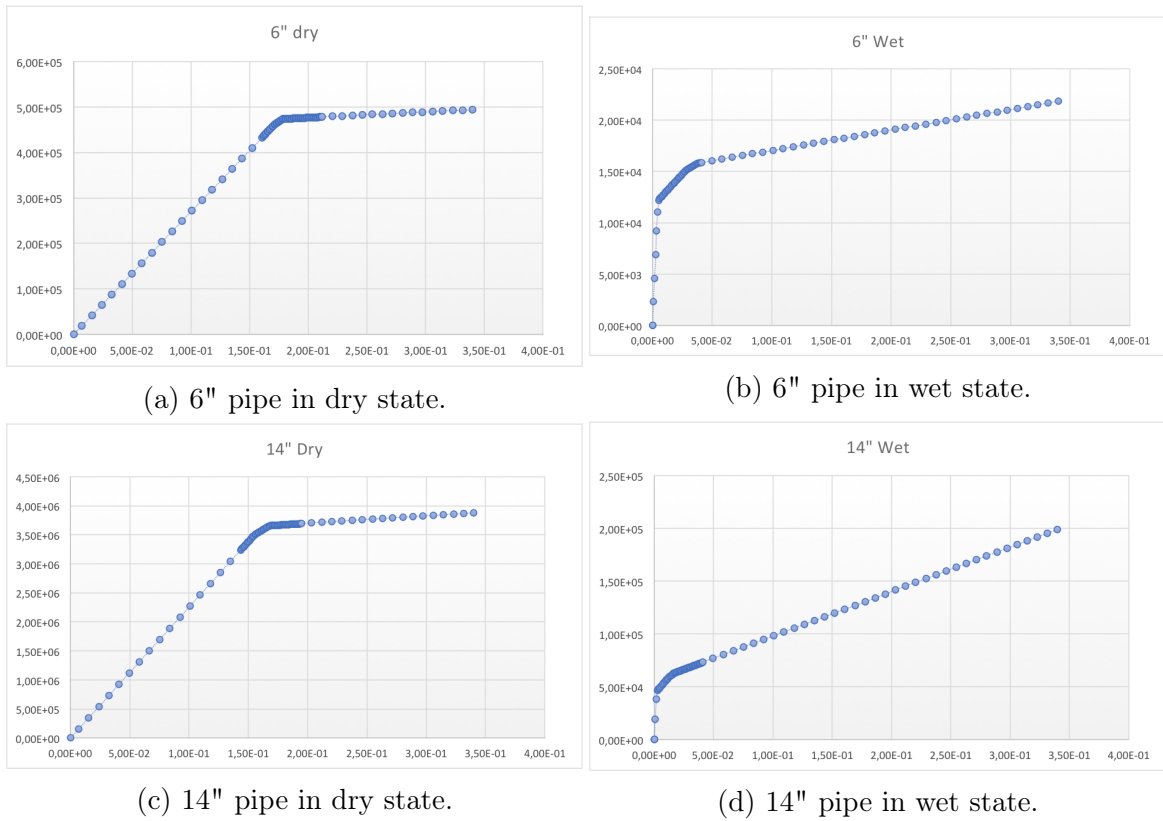
Figure 3.1: Bending Moment vs. Curvature.

Chapter 4

Elastic Case

4.1 Method Elastic Case

To analyse the global behaviour in relation to torsion instability, catenary models of the pipes were made using linear elastic Pipe31 elements. The results from the prestudy (see Section 3.2) were used to describe the material behaviour of the pipes. As the slip curvature was relatively small in wet state, the bending stiffness was given the value of EI_s, under estimating the pipes bending moment capacity. For the dry state, the initial bending moment EI_I was used, assuming that buckling would happen before slip. This would have to be reaffirmed after the analysis.

The friction between the pipes and the sea bottom was set to 0.4 in x-direction and 1.0 in y-direction, while the penetration stiffness was set to $60kN/m^2$. This was simulated by a Coulomb friction model using the contact element type Cont126.

Torsional coupling was turned off, as the pipes otherwise would start rolling on the ground during the analysis. Due to the pipes downward penetration into the soil this would not happen in reality. Drag and external pressure was added to the models using the element type Sea150.

To get to the catenary configuration the pipes were first modelled laying on the sea bottom, and then lifted at one end while being restrained by an axial tension force in the other. This was done in static mode over an illustrating time of 5s.

The bottom tension force T_0, was at the start given a high value to ensure convergence. Then linearly decreased to $1kN$ for the 6" pipes and $3kN$ for the 14" pipes, at the time 5s.

When the catenary configuration was established, both ends were restrained from translational movement. A prescribed rotation around the global z-axis was given at the top end of the pipes, while the bottom end was fixed against torsional rotation. The rotation was increased over a period of 40s (5s-45s) in dynamic mode, until looping occurred.

4.2 Result Buckling Moment Elastic Case

Trying to predict the results, the Greenhill formula was used (See section 1.5.1). The formula is only defined for straight structures, though Neto & de Arruda Martins (2013) shows that it, in most cases, gives sufficiently good results for initial estimates.

A lower bound was established using T_0, while the upper bound was calculated using the maximum tension (over time) slightly above the loop. As one can see from Figure 4.1 the tension has a significant general increase before buckling. This is most likely due to the translational restrain in both ends and friction towards the sea bottom. Consequently the pipe will elongate and lift up from the sea bottom during loop formation.

(a) 6" pipe in dry state.

(b) 6" pipe in wet state.

(c) 14" pipe in dry state.

(d) 14" pipe in wet state
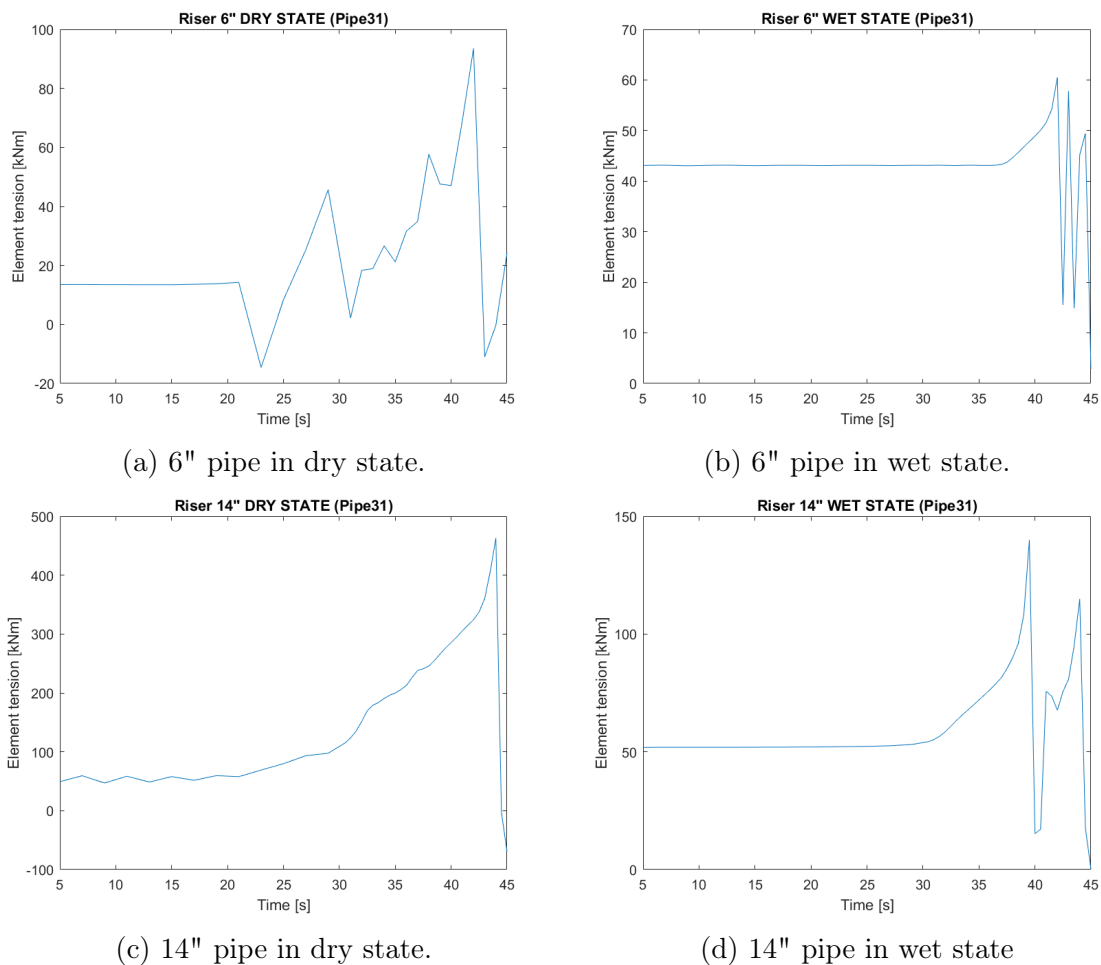
Figure 4.1: Element Tension Above the TDZ Over Time (Pipe31).

As the value of the imposed rotation is increased, the torsion moment is expected to follow suit. This is until buckling where the torsion moment drops, which implys that a loop has been formed. (Neto & de Arruda Martins 2013) (Sævik & Koloshkin 2017)

From Figure 4.2 one sees that buckling happens inside the predicted area, except
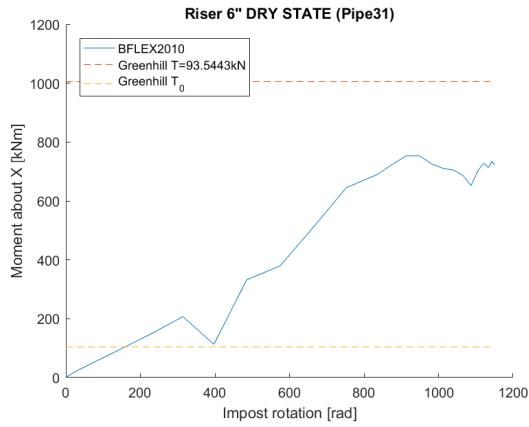
(a) 6" pipe in dry state.
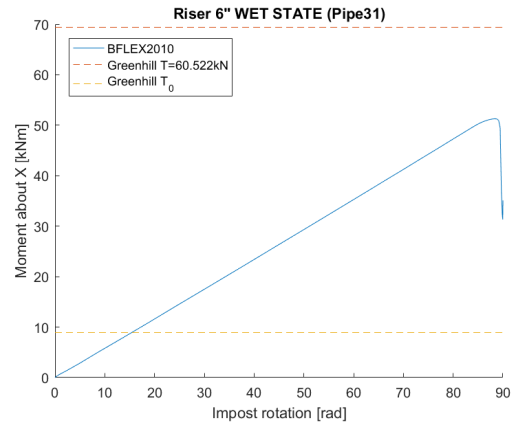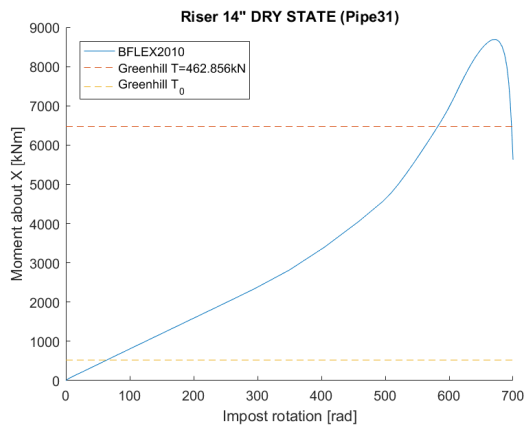
(b) 6" pipe in wet state.

(c) 14" pipe in dry state.
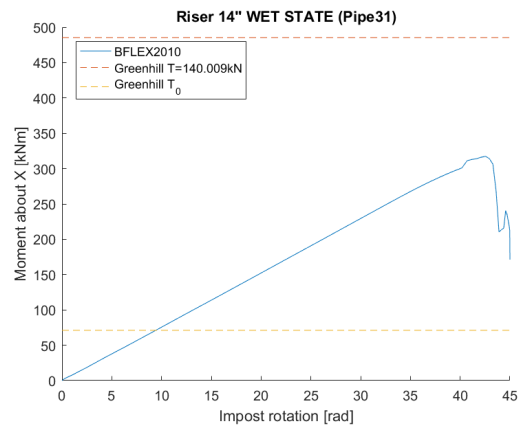
(d) 14" pipe in wet state

Figure 4.2: Buckling Moment (Pipe31) & Greenhill estimate.

for the 14" pipe in dry state. Here the buckling moment is higher than expected. However, the 14" pipe in dry state is very stiff, and this may have an effect on the buckling behaviour. It can also be the experienced buckling length, which is reduced due to the catenary position and stiffness of the pipe. Further, the Greenhill formula is not defined for curved structures, and likewise not meant for structures transitionally restrained at both ends.

On the other hand, it is noticeable that the buckling moment for the pipes in dry state is considerable larger than in wet state. This is to be expected considering the higher value of the bending stiffness.

Taking a look at the 6" pipe in Figure 4.2a, is evident that there is disturbances during the process. Studying the pipe further in x-post, there seems to be wavy formations appearing and disappearing over time along the length of the riser. This might be due to the impost rotation being increased too quickly, or because of the high bending stiffness. It can also be related to the contact action between the pipe and the sea bottom. However, further study is needed to determine the exact cause. In addition, there is no clear reduction in torsion moment suggesting buckling or loop formation for the 6" pipe in dry state. Even so, X-post shows that a loop has formed at time 42s.

The torsion moments in Figure 4.2 is taken from the second to the top element. Looking at an element closer to the loop formation of the 6" pipe in dry state (see Figure 4.3), the disturbances are less evident and only the disturbance during looping remains. Following the looping process in x-post, it becomes evident that the pipe rises significantly form the sea bottom during looping, thus reducing the resistance created by the contact friction.
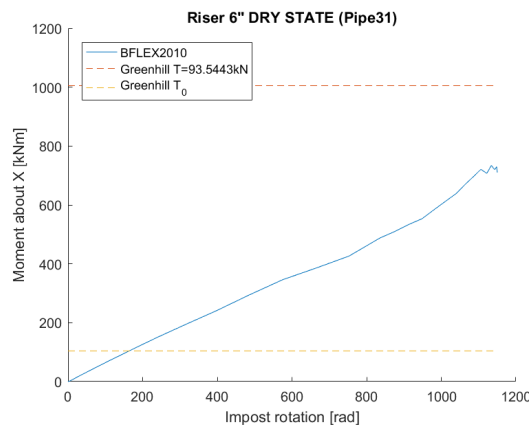
Figure 4.3: Buckling Moment Close to the Loop

4.3 Result Buckling Curvature Elastic Case

The total curvature is determined from the contribution in local y- and z-direction using the formula:

$$\kappa_t = \sqrt{\kappa_y^2 + \kappa_z^2} \tag{4.1}$$

The total curvature along the length of the riser at the time of buckling is shown in Figure 4.4, as well as the maximum allowed curvature (see Subsection 1.4.2) and the resulting slip curvature from the prestudy (see Section 3.2).
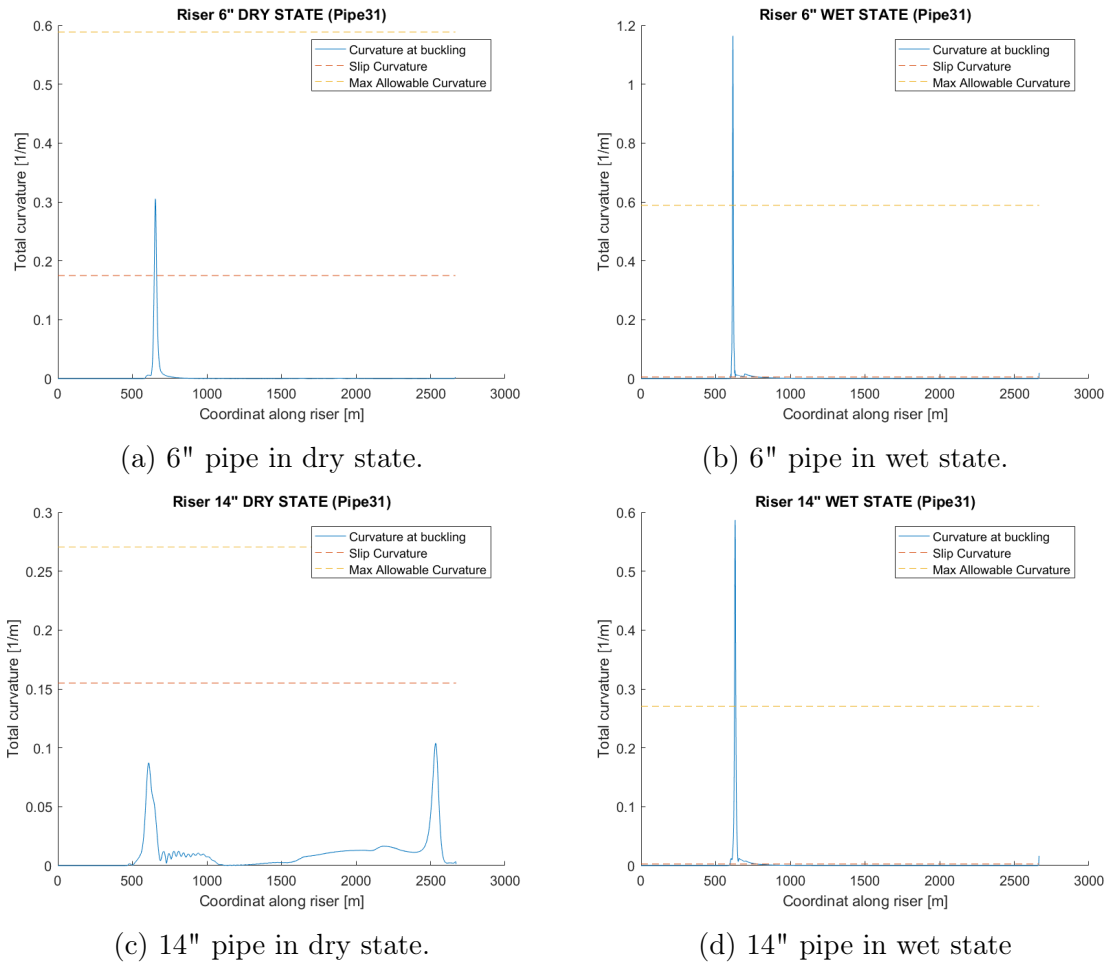

(a) 6" pipe in dry state.

(b) 6" pipe in wet state.

(c) 14" pipe in dry state.

(d) 14" pipe in wet state

Figure 4.4: Total Curvature Along the Length of the Riser (Pipe31).

For the pipes in wet state the buckling curvature is larger than the maximum allowed curvature, implying that buckling will not happen within the regulated limits. However, as EI_s was used as the bending stiffness, under estimating the pipe capacity, this is not certain.

In dry state the buckling curvature is less than the maximum allowed curvature. Though, for the 6", the slip curvature has been exceeded, suggesting that the bending stiffness has been overestimated.

Focusing on the 14" pipe in dry state, there seems to be two loop formations. There is one close to the top and one in TDZ. However, following the process after buckling, only the one in TDZ continues to develop into a kink, while the other straightens out. As can be seen in Figure 4.5.
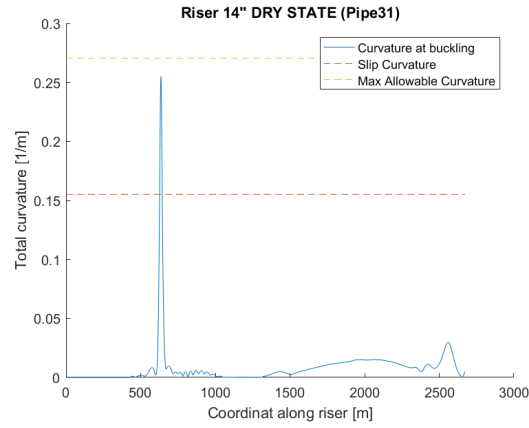
Figure 4.5: Curvature When Kink Has Formed.

Chapter 5

Non-Linear Case

5.1 Method Non-Linear Case

To further study the buckling moment and curvature related to torsion, the same procedure as, in the elastic case, was followed (See Section 4.1). The only difference being that the pipes were modelled using the non-linear element type Compipe42, allowing for the slip behaviour during bending to be taken into account.

Also, to ensure convergence, the pipe was lifted up in catenary position while being held elastic. Then the non-linear effects where smacked into effect at the beginning of the dynamic state process. As a result, the time for which the impost rotation was distributed over was reduced by 0.02s.

5.2 Result Non-Linear Case

In Figure 5.1 the results for the torsion buckling moment is presented along with Greenhill estimates (see Subsection 1.5.1 & Section 4.2). For the estimates in dry state EI_I was used, while in wet state both EI_I and EI_s have been used to create the bounds.

For the dry state, the buckling moment results are relatively similar to the elastic case (See Figure 4.2), while in wet state there is a significant increase.

There are still a lot of disturbances for the 6" pipe in dry state. Studying the process in X-post the disturbances start just as the the loops start forming in the higher regions of the pipe. The forming of these loops creates small shifts of the TDP, which may be the cause of the disturbances seen in Figure 5.1a.

Also, looking at the curvatures in Figure 5.2 versus Figure 4.4, it is clear that the buckling curvature in wet state has decreased. Though, it is still higher than the allowed curvature. Even so, it is now much closer to the allowed curvature, especially
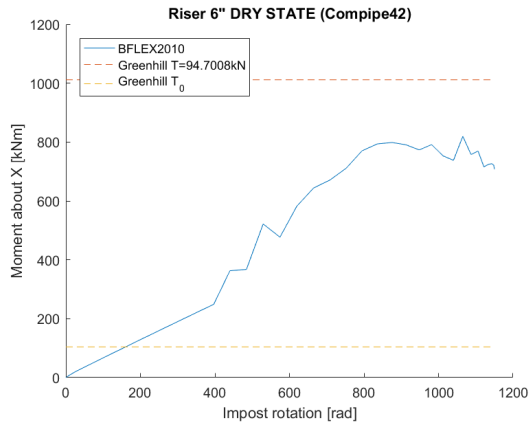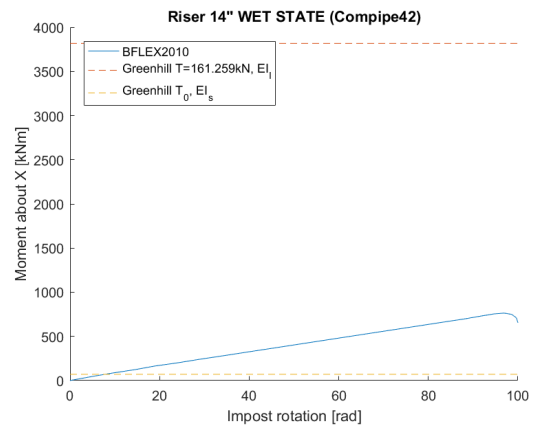
(a) 6" pipe in dry state.
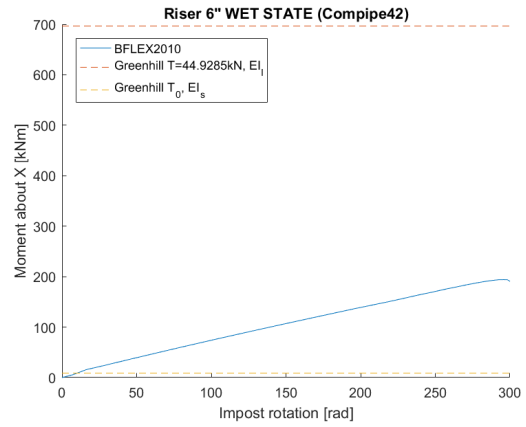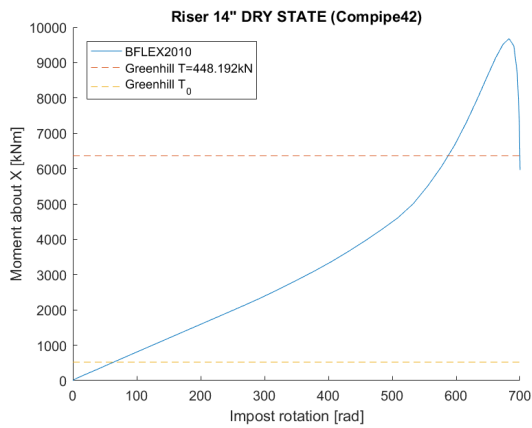
(b) 6" pipe in wet state.

(c) 14" pipe in dry state.

(d) 14" pipe in wet state

Figure 5.1: Buckling Moment (Compipe42) & Greenhill estimate.

for the 6" pipe in wet state. This increases the risk of buckling occurring before allowed curvature has been reached, i.e., due to imperfections or local buckling reducing the capacity.
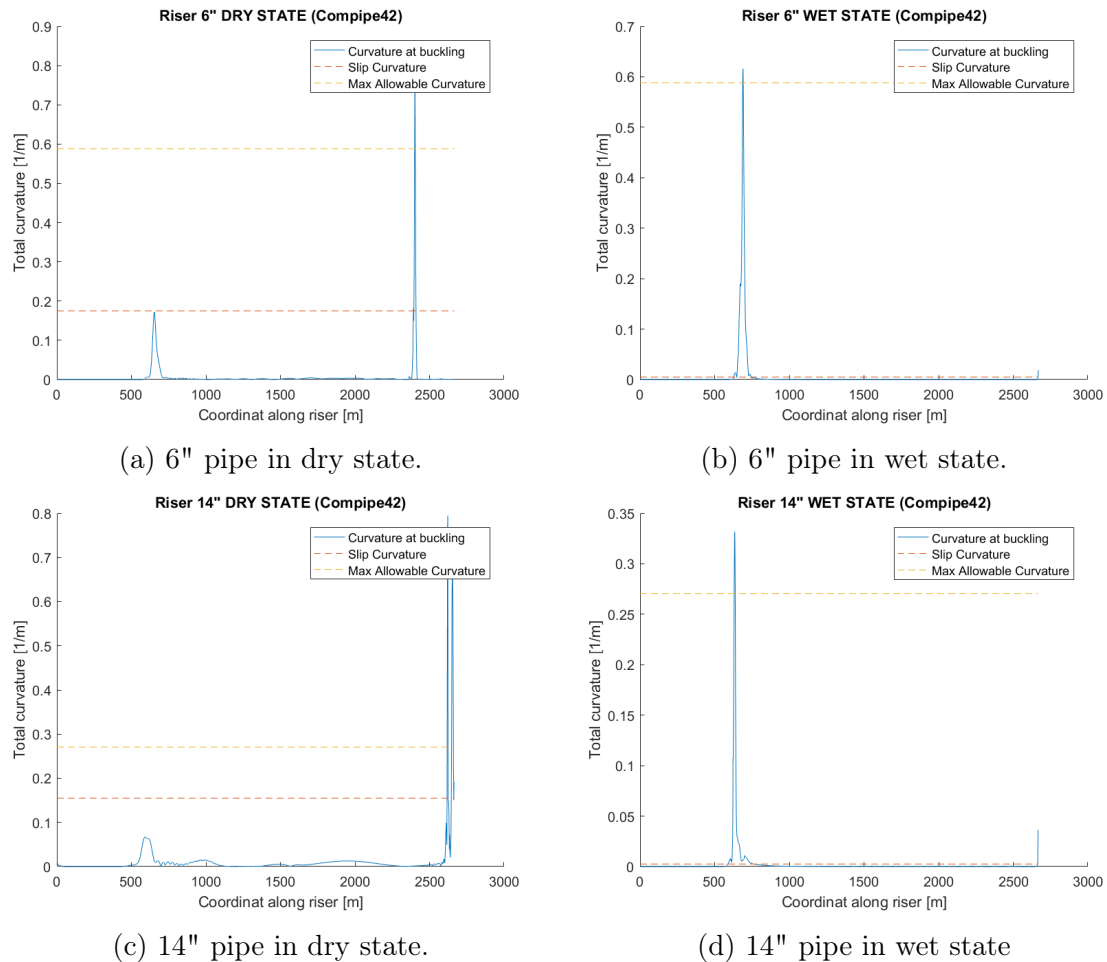

(a) 6" pipe in dry state.

(b) 6" pipe in wet state.

(c) 14" pipe in dry state.

(d) 14" pipe in wet state

Figure 5.2: Total Curvature Along the Length of the Riser (Compipe42).

As for the 14" pipe in dry state, the buckling curvature at TDZ is much the same compered to the elastic case. This is to be expected considering that the buckling curvature at the bottom is less than the slip curvature. However, for the curvature at the top, this is not the case, as it has become much larger. In addition, in the non-linear case, the loop in the top dos not straiten out while the kink at TDZ is formed. The phenomena of loops appearing in the top of the pipe section also seems to be happening for the 6" in dry state using the Compipe42 element type.

Even though there are loops forming in the higher regions of the pipes in dry state, it is important to take note that the value of the impost rotations in these cases are extremely high. Consequently, these rotations will not be nearly as large in reality, and the possibility of this buckling scenario happening is very low. Normally the highest impost rotation in a realistic worst case scenario is about π.

For elastic linear cases the relationship between torsion moment and torque is given by:

$$M_x = \frac{GI}{L_T}\theta_x \tag{5.1}$$

Where L_T is the total length of the pipe that is experiencing the torque. Creating a worst case scenario, setting $\theta_x = \pi$, $L_T = 2000m$ and using the torsion stiffness found in the prestudy (see Section 3.2), one gets the following utilisation of the buckling moment as presented in Table 5.1. The utilisation is quite small, and one may conclude that looping due to only torque for a catenary formation at this water dept, is unlikely.

Table 5.1: Utilization of Torsion Buckling Moment

	$GI[MNm^2]$	$M_x[kNm]$	$M_{x,crit}[kNm]$	$\frac{M_{x,}}{M_{x,crit}}[\%]$
6" Dry	1.59	2.50	730	0.34
6" Wet	1.59	2.5	194	1.29
14" Dry	20.9	32.8	9680	0.34
14" Wet	20.7	32.5	764	4.26

Chapter 6

Dynamic Heave Scenario

6.1 Method Dynamic Heave Scenario

Due to wind and waves, the supporting/installing vessel of the riser will not be still. This will have an effect on possible creations of loops, i.e: reduced tension due to downward motion, or the interaction effects from shifts of the TDP.

To simulate these effects, an analysis was made using pipes with built in torque and subjecting them to a heave motion. The models were put up using the same procedure as for the cases in Chapter 4 & 5, for the start. The imposed rotation was reduced to different percentage of the critical torque found in Section 4.2 (dry state) & 5.2 (wet state). Then the pipes where subjected to a heave motion over 30s (time: 45s - 75s), following the formula:

$$A = A_0 \sin(\frac{2\pi}{T_h}(t - t^*)) \tag{6.1}$$

Where A_0 is the amplitude, T_h is the period, t is the time $\in$ [45s, 75s] and t^* is the time at which the heave motion starts (45s). In this analysis T_h was set to 10s for all cases, resulting in 3 complete oscillations.

For this analysis there have been used five amplitudes: 0.5m, 1m, 2m, 3m, 4m and 5m, in combination with three levels of utilisation of the critical torque: 25%, 50% and 75%.

When it comes to choice of element type for the pipes, the element type Compipe42 was used for the pipes in wet state. For the pipes in dry state Pipe31 was used as slip effects are negligible in this case (see Section 5.2), and to speed opp the analysis.

6.2 Result Dynamic Heave Scenario

The maximum total curvature at the TDZ over time for the 6" pipe in wet state is presented in Figure 6.4. It is noticeable that in all cases the total curvature has a

general increase over time. In addition, the torsion moment seem to decrease.

(a) Angle nr. 1   (b) Angle nr. 2
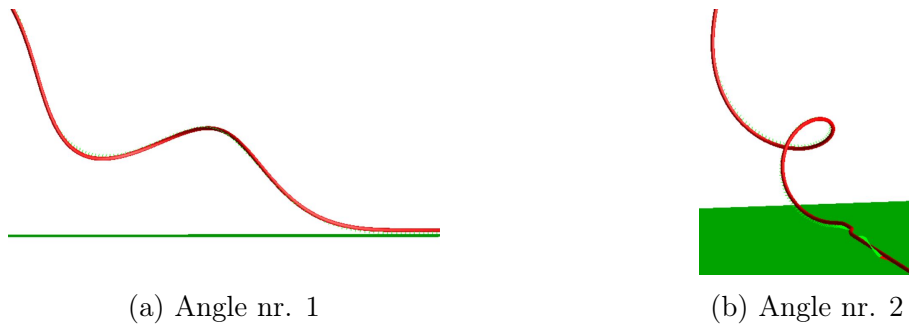
Figure 6.1: 6" Pipe in Wet State, 75% Torque Utilisation, A_0=4m, t=45s.

In the cases of 50% and 75% utilisation of the torque, the pipe buckles as the total curvature exceeds the buckling curvature (see Figure 6.2). For the 75% utilisation cases the pipe's curvature strictly increases from 5s until 75s. As one can see in Figure 6.1, the deformation is quite large, even before the heave oscillations start.

(a) Angle nr. 1   (b) Angle nr. 2

Figure 6.2: 6" Pipe in Wet State, 50% Torque Utilisation, A_0=4m, t=70s.

Note that the increase in maximum total curvature for the 6" pipe in wet state experiencing a 0.5m amplitude is larger than that of the pipe experiencing a 0.4m amplitude, in the case of 50% torque utilisation (eee Figure 6.4d). The same goes for the 14" pipe in dry state. However, this is not the same for the 14" pipe in wet state (see Figure 6.5d & 6.7d).

Taking a closer look at the interaction process between the pipe and the sea bottom during heave oscillations (45 s-75 s), the pipes seem to create local rise ups, as seen in Figure 6.3. These rise ups seems to decrease the buckling resistance. In the case where the rise up is not straightened out again until the next upward heave motion, the reduction in friction force seems to accelerate the buckling process. It is also noticeable that the TDP has a significant shift in transverse direction after touch-down, signifying higher possibility of loop formation.

For the 14" pipe the looping happens before the heave motion is applied in both states when there is 75% utilisation. This can be seen in Figure 6.5f & 6.7f, as the maximum total curvature at the TDZ is larger than critical curvature at 45s. Most
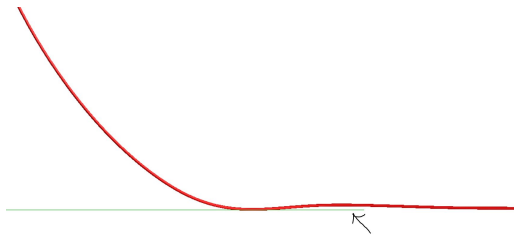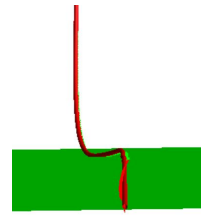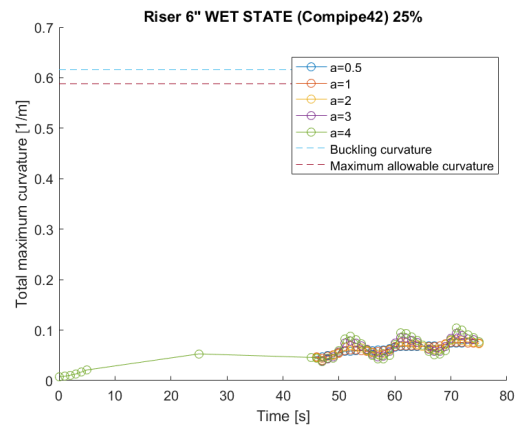
(a) Angle nr. 1   (b) Angle nr. 2

Figure 6.3: 14" Pipe in Wet State, 25% Torque Utilisation, A_0=4m, First Touch Down.
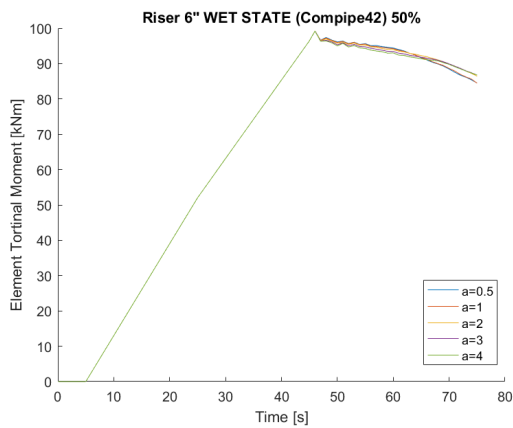
likely this is a result of how fast the impost rotation has been applied, affecting the pipe's critical torque (see Chapter 5 & 4).
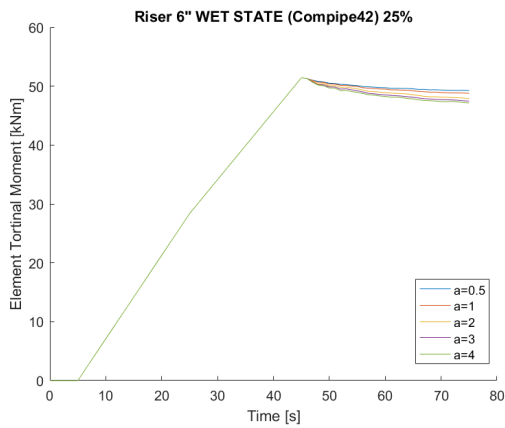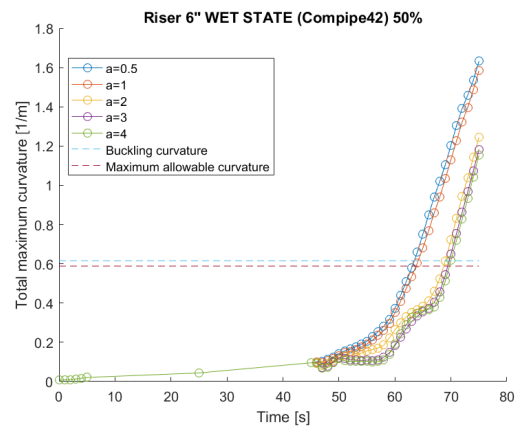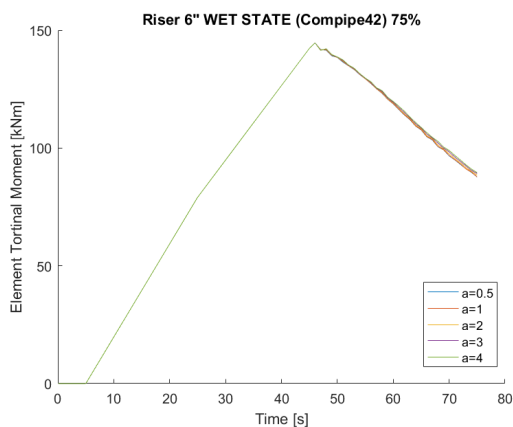
(a) Torsional moment, 25% utilisation.

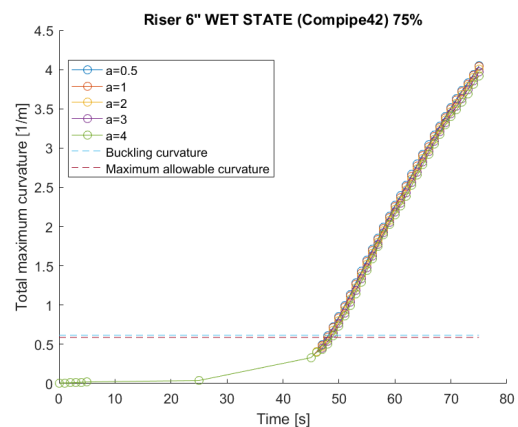(b) Maximum curvature, 25% utilisation.

(c) Torsional moment, 50% utilisation.
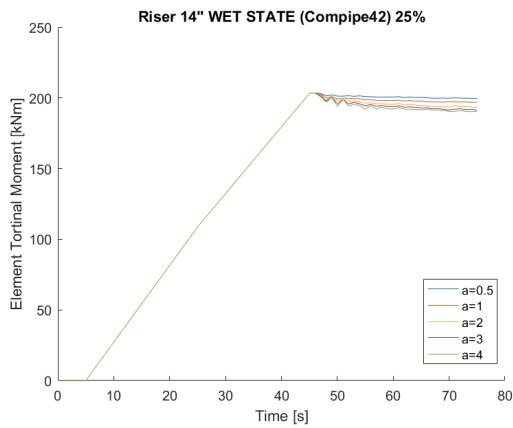
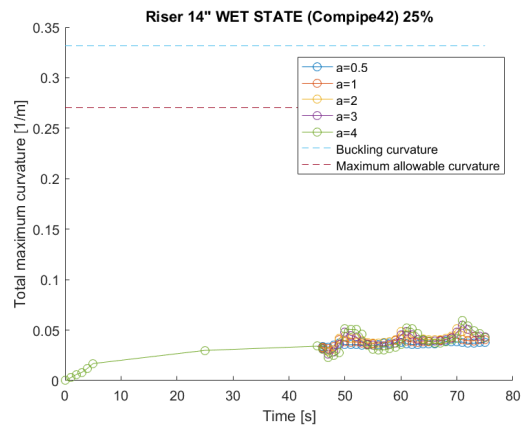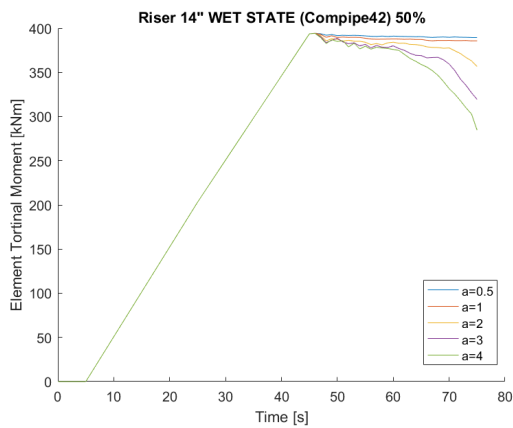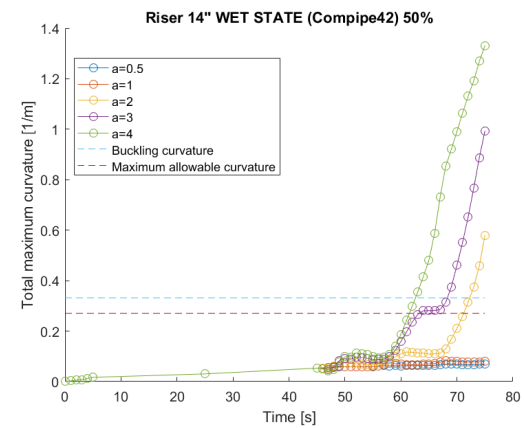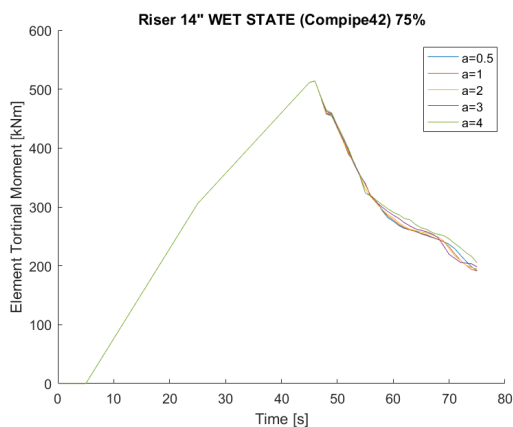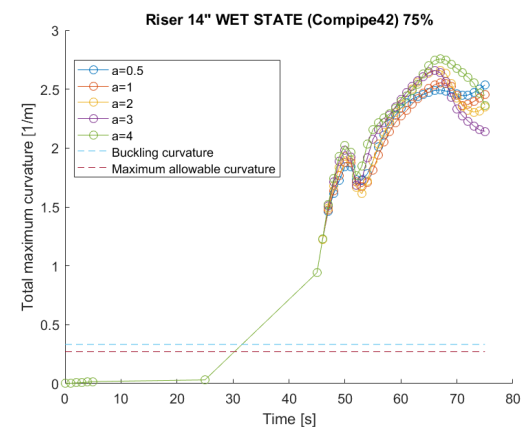(d) Maximum curvature, 50% utilisation.

(e) Torsional moment, 75% utilisation.

(f) Maximum curvature, 75% utilisation.

Figure 6.4: 6" Pipe in Wet State: Torsional Moment and Total Maximum Curvature at the TDZ Versus Time.

(a) Torsional moment, 25% utilisation.

(b) Maximum curvature, 25% utilisation.

(c) Torsional moment, 50% utilisation.

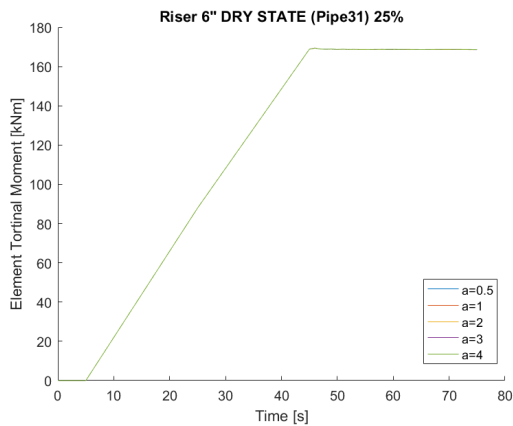(d) Maximum curvature, 50% utilisation.

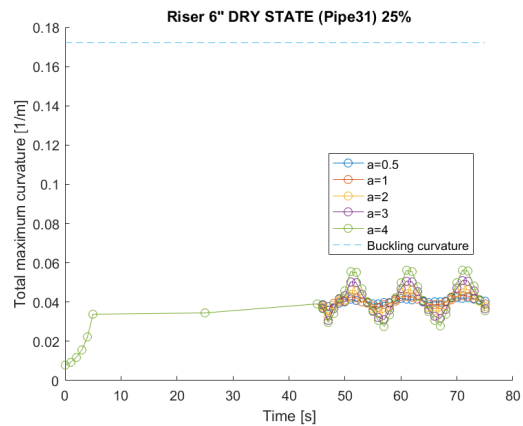(e) Torsional moment, 75% utilisation.
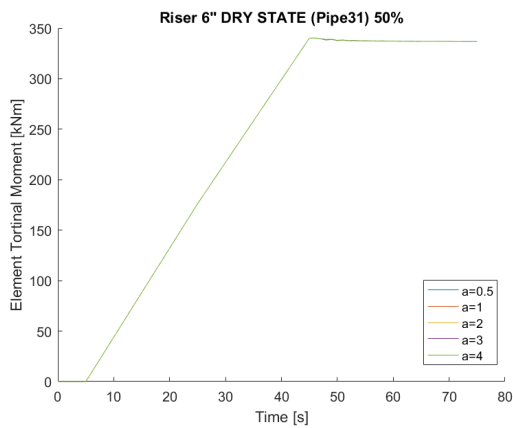
(f) Maximum curvature, 75% utilisation.

Figure 6.5: 14" Pipe in Wet State: Torsional Moment and Total Maximum Curvature at the TDZ Versus Time.
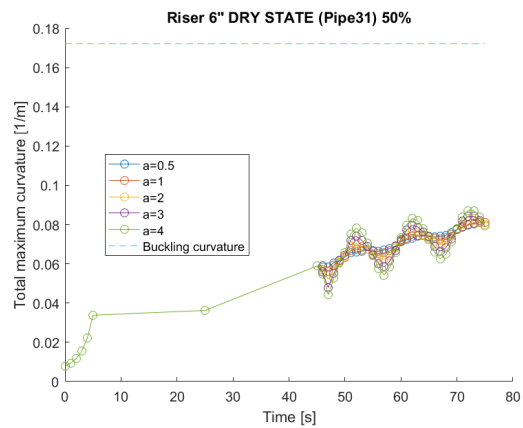
(a) Torsional moment, 25% utilisation.

(b) Maximum curvature, 25% utilisation.

(c) Torsional moment, 50% utilisation.

(d) Maximum curvature, 50% utilisation.

(e) Torsional moment, 75% utilisation.

(f) Maximum curvature, 75% utilisation.

Figure 6.6: 6" Pipe in Dry State: Torsional Moment and Total Maximum Curvature at the TDZ Versus Time.

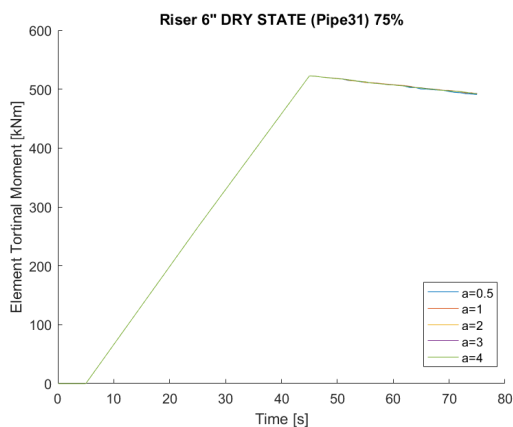(a) Torsional moment, 25% utilisation.

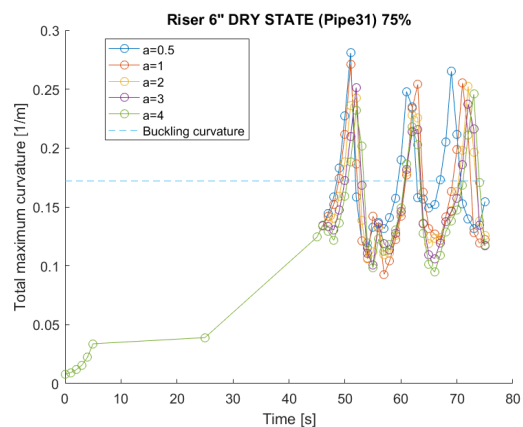(b) Maximum curvature, 25% utilisation.

(c) Torsional moment, 50% utilisation.
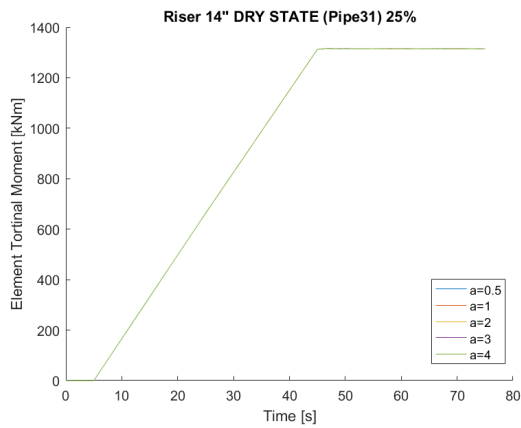
(d) Maximum curvature, 50% utilisation.
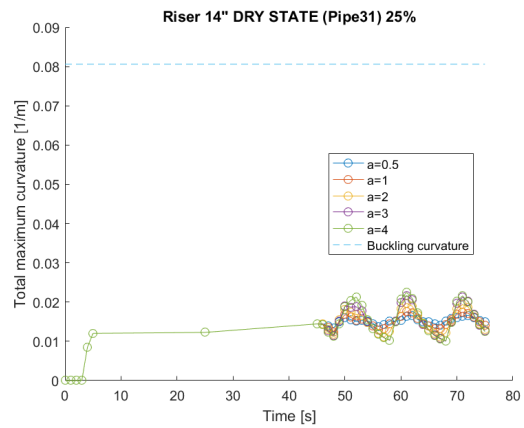
(e) Torsional moment, 75% utilisation.
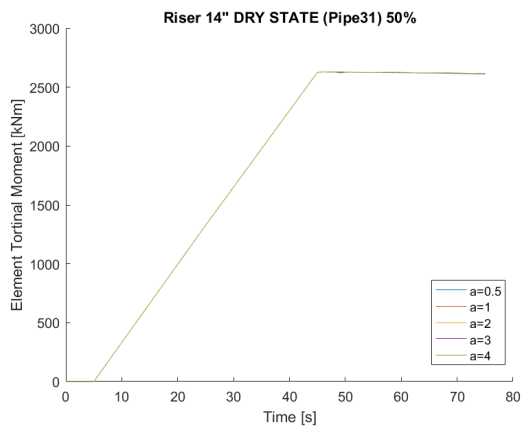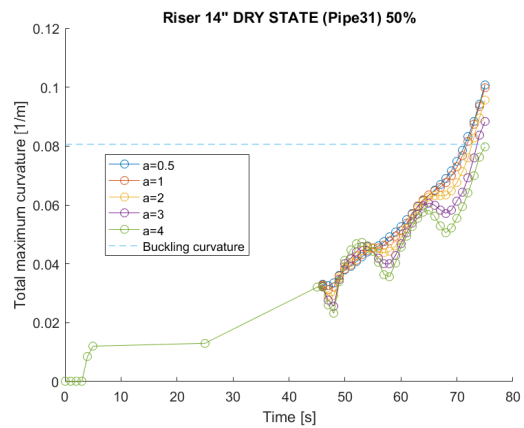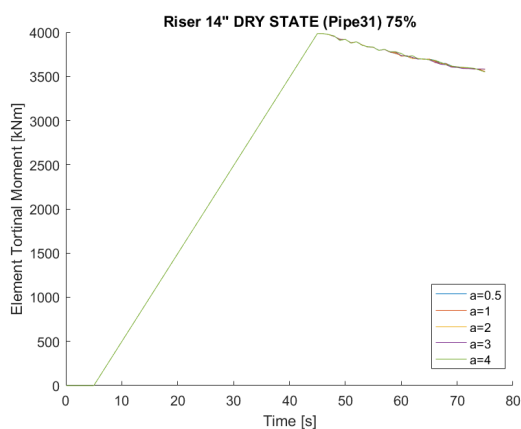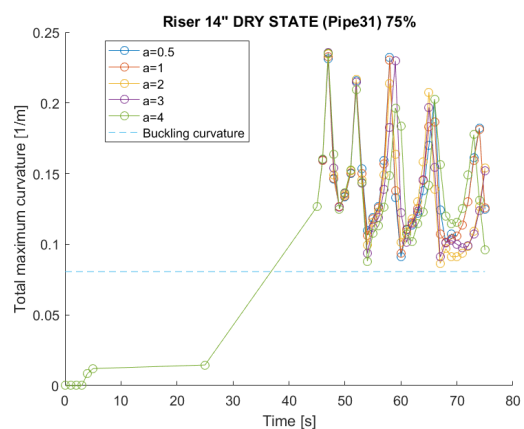
(f) Maximum curvature, 75% utilisation.

Figure 6.7: 14" Pipe in Dry State: Torsional Moment and Total Maximum Curvature at the TDZ Versus Time.

Chapter 7

Extended Dynamic Heave Scenario

7.1 Method Extended Dynamic Heave Scenario

From the dynamic heave scenario analysis, it becomes apparent that the maximum total curvature at the TDZ has a general increase (see Section 6.2). To further study this phenomena for a more realistic imposed rotation with a value of π, an extended dynamic heave scenario analysis was done for the pipes in wet state. The setup is the same as the dynamic heave scenario (see Section 6.1, with the exception of the length of time the heave motion is applied. Instead of over 30s (45s-75s), the heave motion is now applied over 100s (45s-145s), allowing for ten complete oscillations. The analysis was preformed with the amplitudes: 0.5m, 2m and 4m.

7.2 Result Extended Dynamic Heave Scenario

Seen from Figure 7.2 & 7.3 the tendency of increasing maximum total curvature is declining. The same goes for the decreasing torsion moment (See Figure 7.1). This means that for small imposed rotations where buckling does not occur, the torsion moment and the maximum total curvature will stabilise.
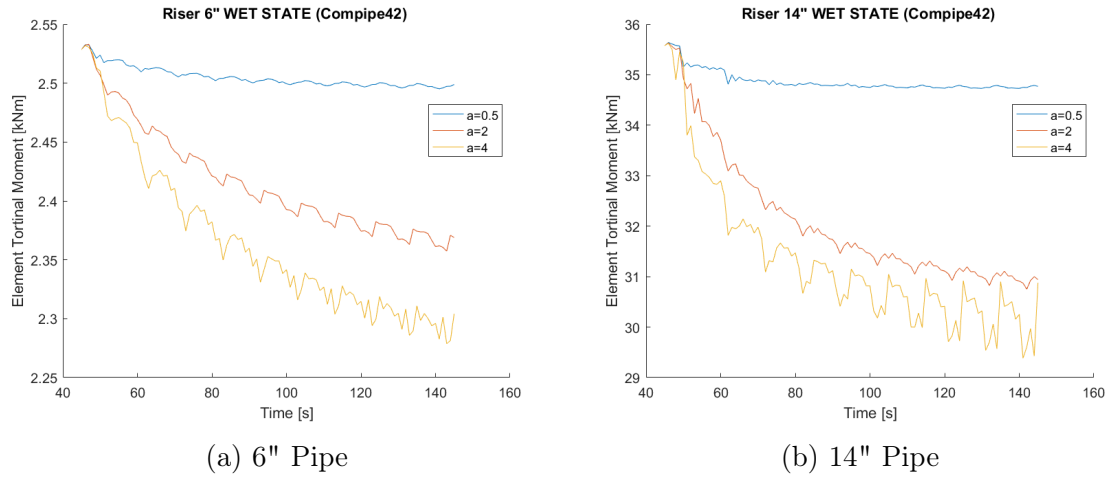
(a) 6" Pipe

(b) 14" Pipe

Figure 7.1: Torsional Moment vs. Time.

(a) 6" Pipe

(b) 14" Pipe
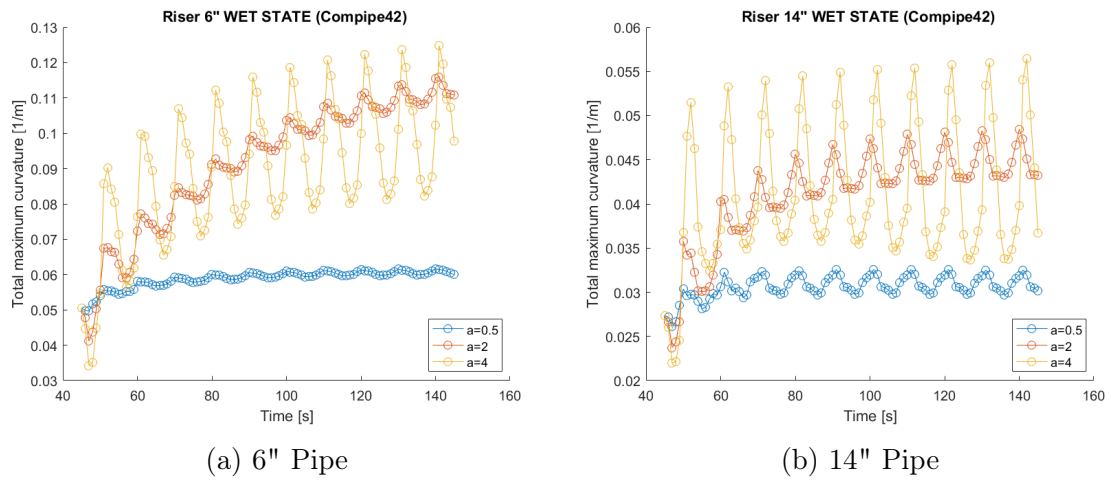
Figure 7.2: Maximum Total Curvature vs. Time.

(a) 6" Pipe

(b) 14" Pipe

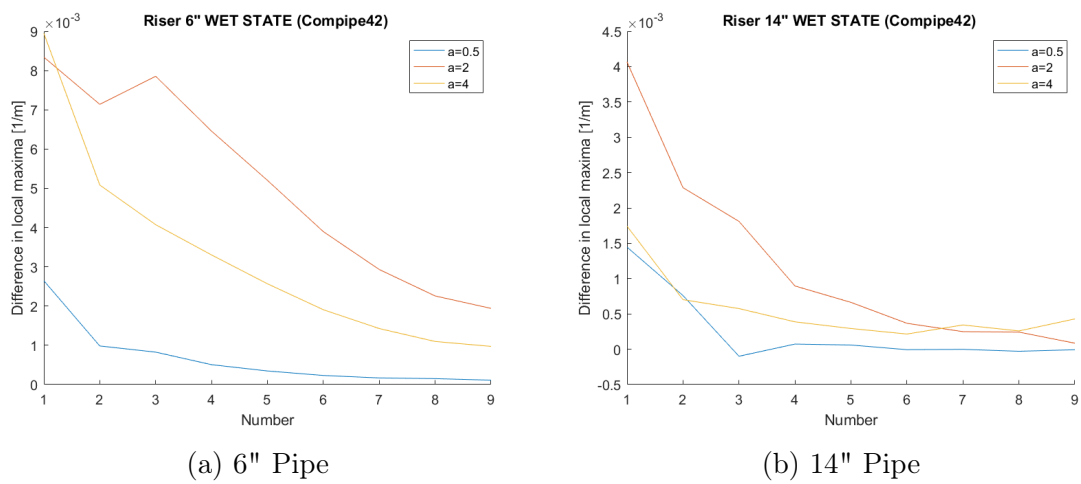Figure 7.3: Difference in Local Maximum of Maximum Total Curvature.

Chapter 8

Local Effects in Heave

8.1 Method Local Effects in Heave

A calculation of total minimum critical external pressure end cap load (see Equation 1.38) for the inner tensile armour layer of the pipes in wet state, are presented in Table 8.1.

Table 8.1: Minimum Critical External Pressure End Cap Load for a Tendon.

Pipe	n	α[rad]	R_h[m]	GJ[Nm^2]	EI$_2$[Nm^2]	EI$_3$[Nm^2]	P[kN]
6"	52	0.457276	0.099	7.29	4.725	52.5	49.21
14"	70	0.549779	0.219	25.92	16.8	231	69.65

An approximation of the end cap load on a tendon P due to external pressure, is given by the correlation:

$$\rho_w g h * \pi R_y^2 = nP \tag{8.1}$$

Where ρ_w is the density of the water, h is the water depth, R_y is the outer radius of the pipe cross-section and n is the number of tensile armour layers. Using the two geometries and a water depth of 2000m, the result becomes as presented i Table 8.2.

Table 8.2: Approximate External Pressure End Cap Load on a Tendon

Pipe	$\rho_w[kg/m^3]$	h[m]	R_y[m]	n	P[kN]
6"	1024	2000	0.1115	2	392.35
14"	1024	2000	0.2380	2	1787.61

Compering the two tables, Table 8.1 & 8.2, it becomes evident that the end cap load in both cases are well over the critical value, suggesting that the pipes are not designed for such a deep water depth. The water depth is therefore reduced to 400m for the 6" pipe, which is right below critical level. For the 14" pipe the water depth is first set to 100m, which is under critical, and then to about critical level at 370m.

8.1.1 Test model

To include the local effect of possible lateral buckling on global torsion instability, a more advanced model of the pipe section is needed. A test section of 1m = 1 element length is made to ensurer that the model has the desired attributes. Only the wet state has been modelled in concern of local effects.

There are five elements used to model the pipe cross-section. Firstly a Compipe42 element is used to cover the bending, pressure and weight attributes. Then two Hshear363 elements of type Shear2helix and with Rectangular geometry type have been used to model the two tensile armour layers. Each representing a single wire in its respective layer, that's effect has been multiplied to simulate the helix as a whole. Further, a Hshear363 element has been used to model the anti-buckling tape. The element is also of type Shear2helix and with geometry type Tape. Lastly the outer-sheet is represented by a Shearhelix type Hshear363 element of geometry type Tube. All the elements are connected by sharing the same end nodes and for the Hshear elements they also share the same radial node.

In regards to material models the Compipe42 element uses the same resultant based model used in the previous presented analysis, only now the axial and torsional stiffness has been reduced to a negligible value. For the inner layer of the tensile armourer an Epcurve with float stress corresponding to the critical end cap load presented in Table 8.1, has been used. While the remaining structural elements have been given elastic material models.

First, the test section is placed at the seabed and then linearly exposed to the external pressure over 4 seconds until actual value, while the ends are restrained against torsional movement.
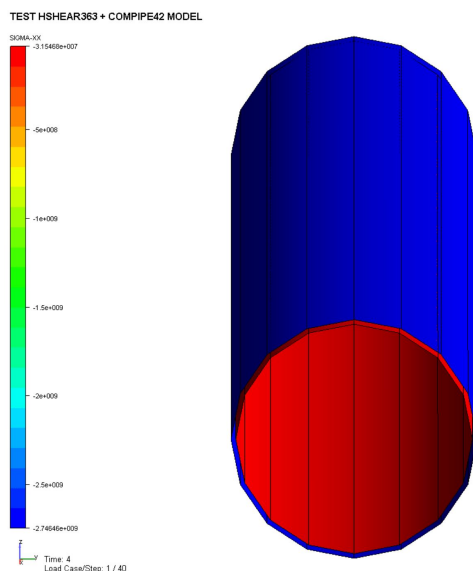

Figure 8.1: Test Pipe 6": Local stress in the tensile armour layers at time 4s.
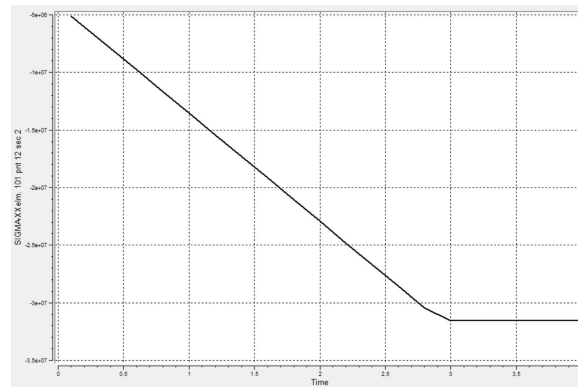
Figure 8.2: Test Pipe 6": Local stress over time in inner tensile layer.

As one can see in Figure 8.2 the stress in the inner tensile layer flattens out as the critical value is reached, forcing the outer tensile to carry the remaining load.

8.1.2 Global model

In the global model, the TDZ is modelled with the element sett used in the test section, while the rest of the pipe is modelled by only Compipe42 elements. As the depth has been changed the bending analyses (see Chapter 3) is done again, this time using a tension of 15kN instead of 50kN and 70kN. The new results of the bending test is presented in Figure 8.3.
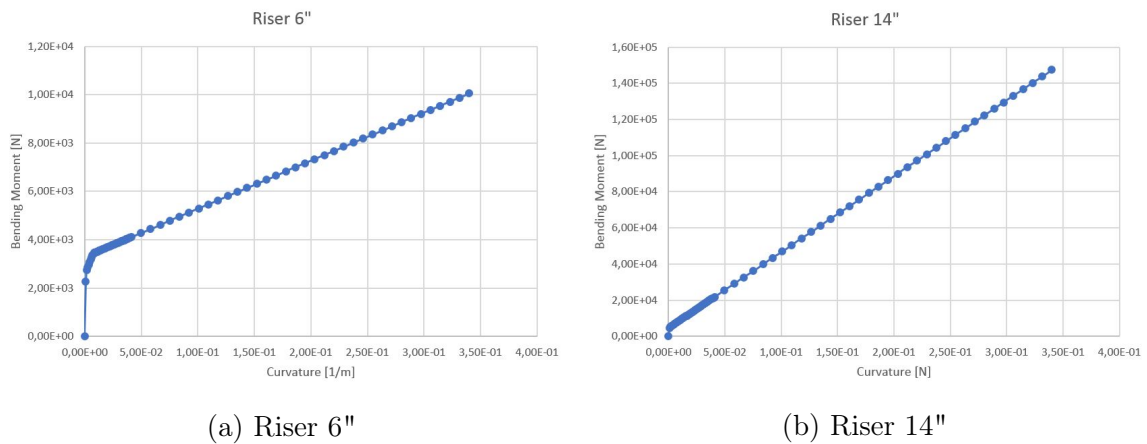
(a) Riser 6"

(b) Riser 14"

Figure 8.3: Result new bending test.

The pipe is modelled lying on the seabed and then lifted at one end over 5 seconds into catenary configuration, while being restricted against torsional movement at both ends. This is done in static domain. Friction, drag and external pressure is simulated as in the previous global models.

After being lifted into catenary position the pipe is given a prescribed hive motion at

the top end following function 6.1, with a period of 10 seconds and an amplitude of 2 or 4 meters. This i done over a time of 1000 seconds, resulting in 100 oscillations. During the oscillating stage the bottom end is fixed against translation.

8.2 Result Local Effects in Heave

For the 6" pipe, in all cases, the curvature and torsion moment seem to stabilise after a few oscillations (See Figure 8.4), and there are no kink formations. Also from Figure 8.5 it becomes evident that critical stress is reached at some point, indicating that local lateral buckling will occur. In the case of the 2m oscillation amplitude, the differences in stress between the inner tensile armour layer and the outer tensile armour is smaller than for the case of 4m amplitude. This suggest that the larger waves increase the imbalance between the layers, resulting in larger torsion of the pipe.

In the case of the 6" pipe exposed to the 4m heave amplitude motion, there seems to be a resonance phenomena with a low frequency oscillation on top of the hive oscillation. This disturbance is also visible in the results for axial stress and bending moments (see Figure 8.5b, 8.6b & 8.6d). Studying the pipe in X-post it becomes apparent that the low frequency oscillation is the pipe switching between bending out positively or negatively around the local z-axis at contact with the seabed. This type of Eigenfrequency may occur during calculations with single sinus wave, but will not happen in reality.

In most cases the forces and moments seem to stabilise. Even so, the bending moment around the local z-axis for the 14" pipe at 100m water depth, does not stabilise (see Figure 8.9). In these cases there are instead a significant steady increase in moment. It is hard to say if this increase will continue, and eventually have an effect on the curvature. On top of this the tensile armour axial stress for the inner and outer layer, is moving towards each other (see Figure 8.5). This suggests that while the solution for the 6" pipe is stable, the under critical 14" pipe is not. However, it is worth taking notice that the most unstable case is that of the 2m amplitude oscillation, which is the only case where buckling does not occur. Another fact to take note of is that for the 14" pipe, the anti-birdcaging tape has the same direction of lay-angle as the outer tensile armour, which is known to reduce torsion resistance.

Looking closer on the torsion unbalance in the under critical case of the 14" pipe subjected to 2m amplitude waves, the inner tensile layer have not reached its maximum capacity. This allows for an increase, resulting in this case, that the pipe turns the opposite way of the expected torsion direction of lateral buckling failure. Consequently, the pipe builds up a natural resistance to the type of global torsion buckling that come as a result of local lateral buckling.

Lastly, considering the 14" pipe at critical water depth, the solution appears stable like the 6" pipe. In this case also, there are no kink formations.

(a) Maximum Total Curvature vs. Time.   (b) Torsion Moment at TDZ vs. Time
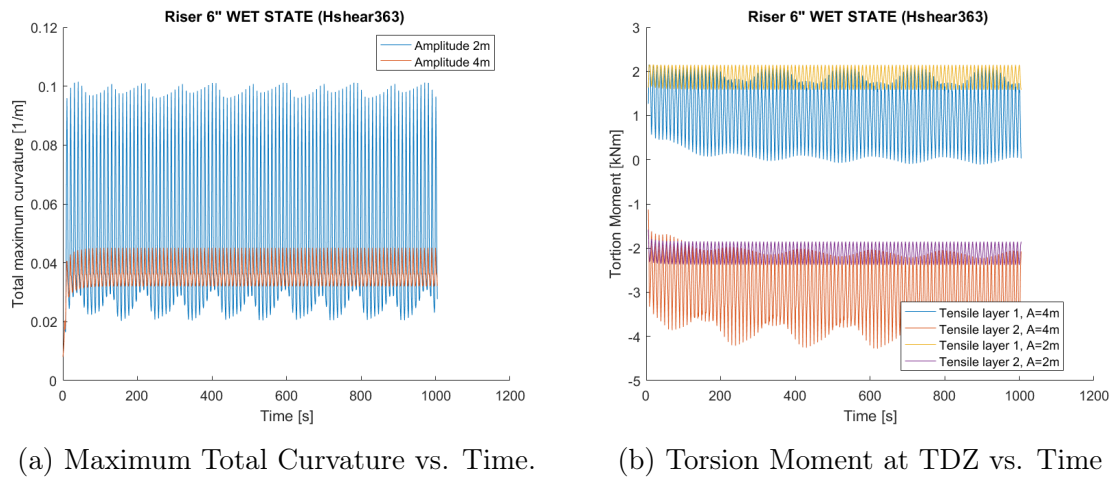
Figure 8.4: Riser 6", h=400: Curvature and Torsion Moment

(a) Amplitude 2m
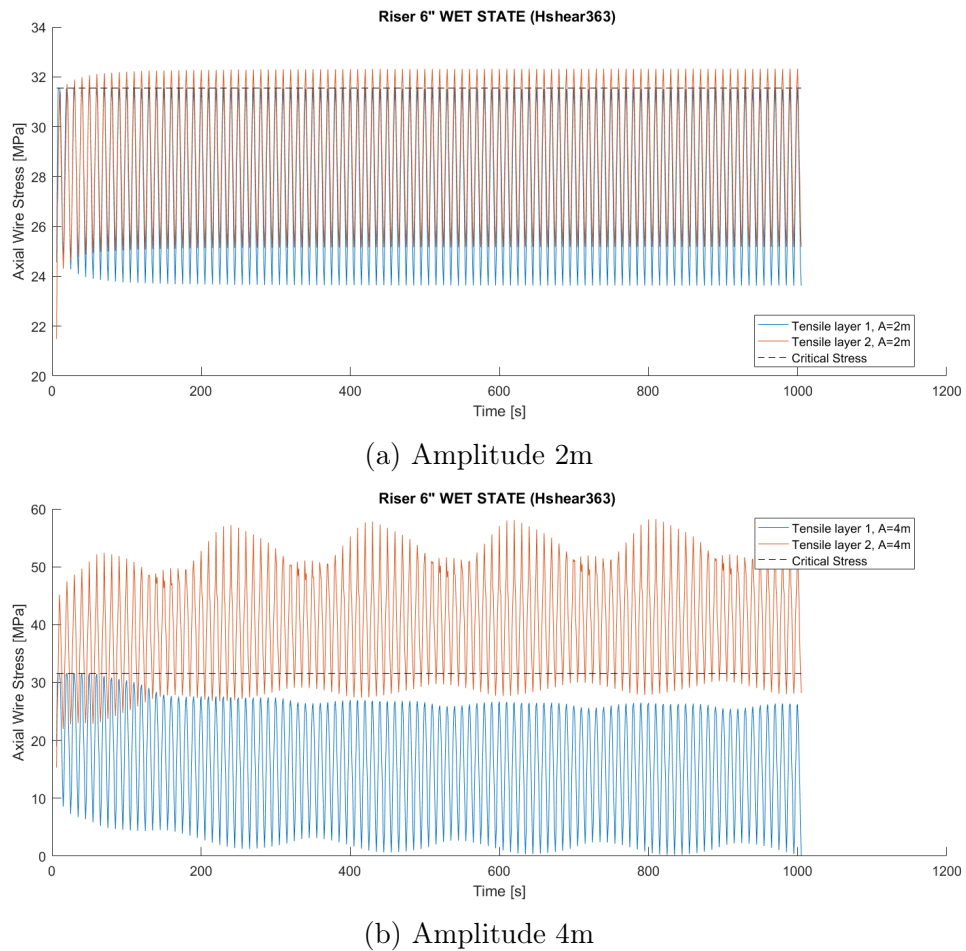
(b) Amplitude 4m

Figure 8.5: Riser 6", h=400: Axial Wire Stress at TDZ vs. Time.

(a) Bending Moment About y, A=2m

(b) Bending Moment About y, A=4m

(c) Bending Moment About z, A=2m

(d) Bending Moment About z, A=4m
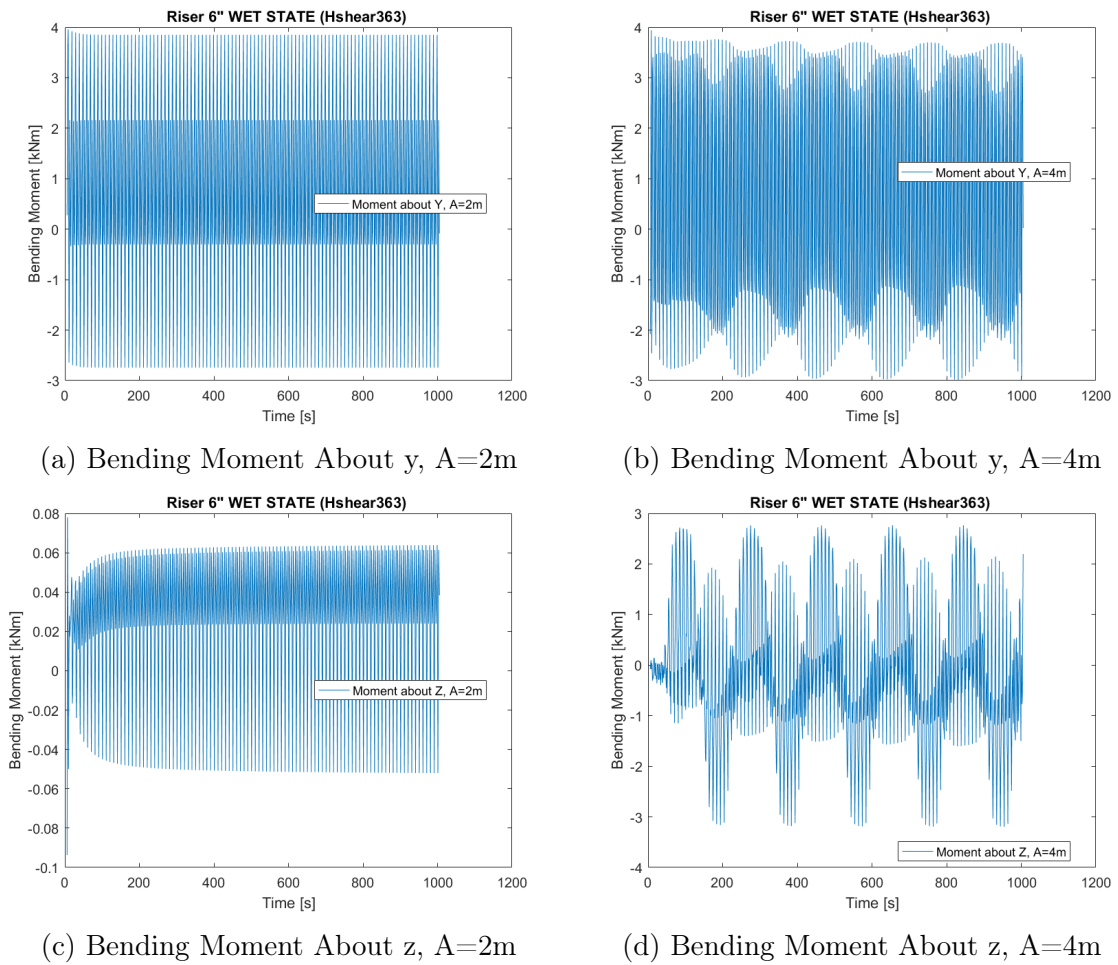
Figure 8.6: Riser6", h=400m: Bending Moment at TDZ vs. Time.

(a) Maximum Total Curvature vs. Time.

(b) Torsion Moment at TDZ vs. Time

Figure 8.7: Riser 14", h=100m: Curvature and Torsion Moment

(a) Amplitude 2m

(b) Amplitude 4m

Figure 8.8: Riser 14", h=100m: Axial Wire Stress at TDZ vs. Time.

(a) Bending Moment About y, A=2m   (b) Bending Moment About y, A=4m

(c) Bending Moment About z, A=2m   (d) Bending Moment About z, A=4m

Figure 8.9: Riser14", h=100m: Bending Moment at TDZ vs. Time.

(a) Maximum Total Curvature vs. Time.   (b) Torsion Moment at TDZ vs. Time

Figure 8.10: Riser 14", h=370m: Curvature and Torsion Moment
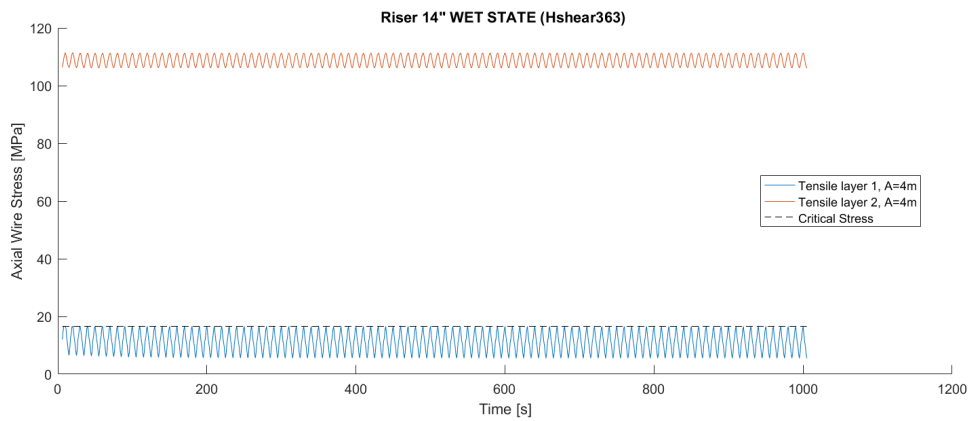
(a) Amplitude 2m

(b) Amplitude 4m

Figure 8.11: Riser 14", h=370m: Axial Wire Stress at TDZ vs. Time.
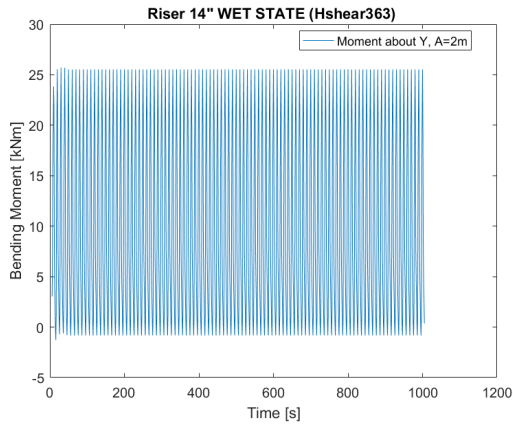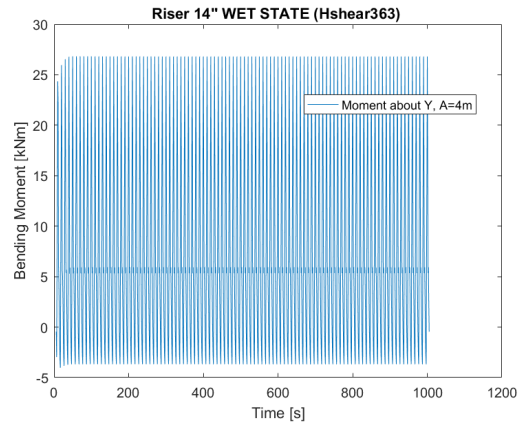
(a) Bending Moment About y, A=2m

(b) Bending Moment About y, A=4m
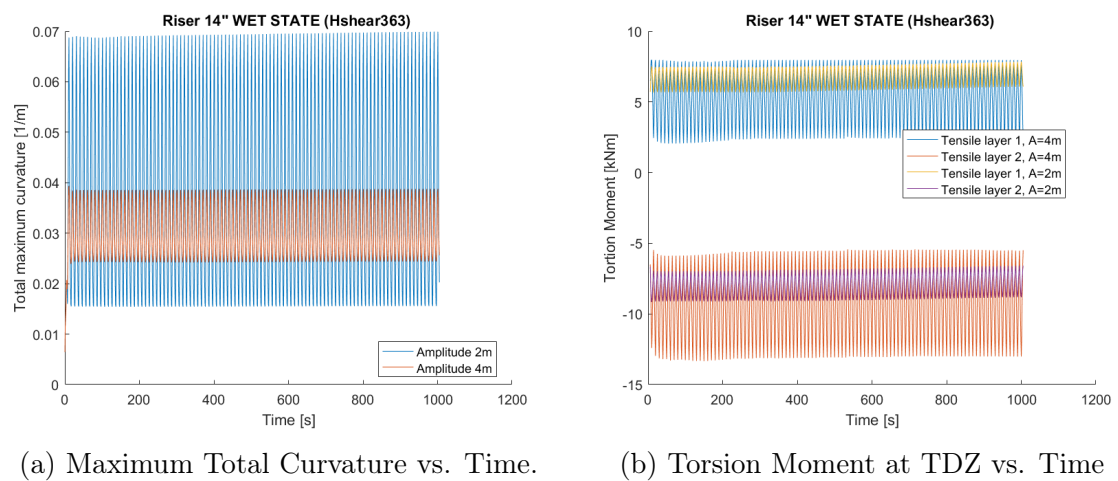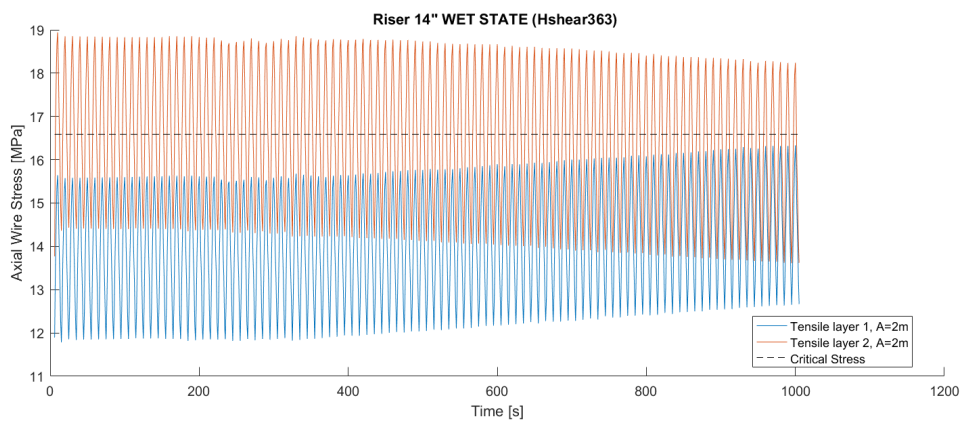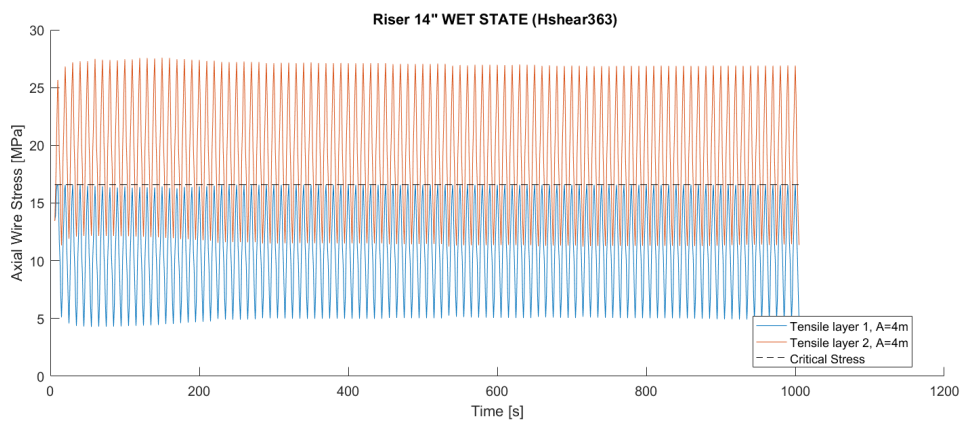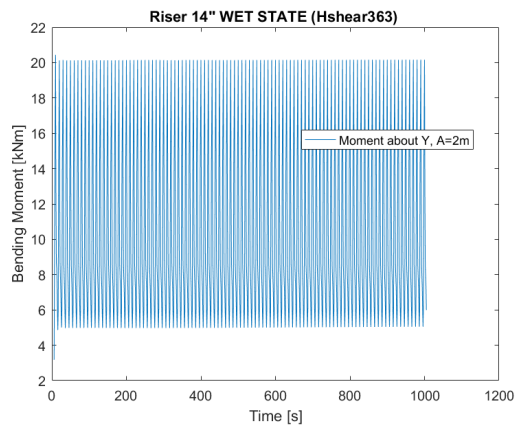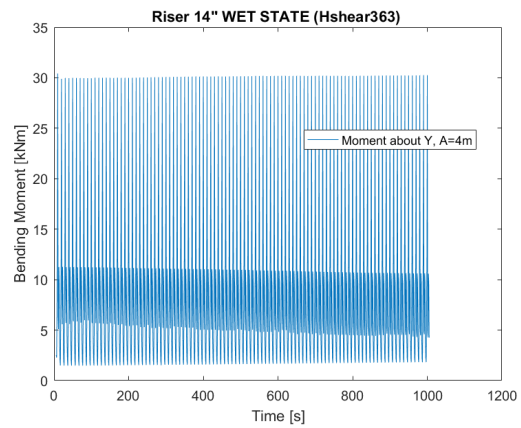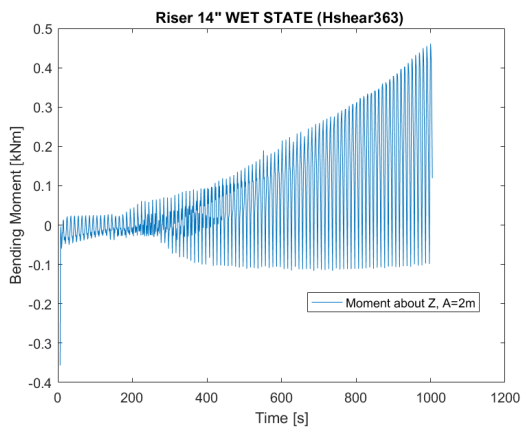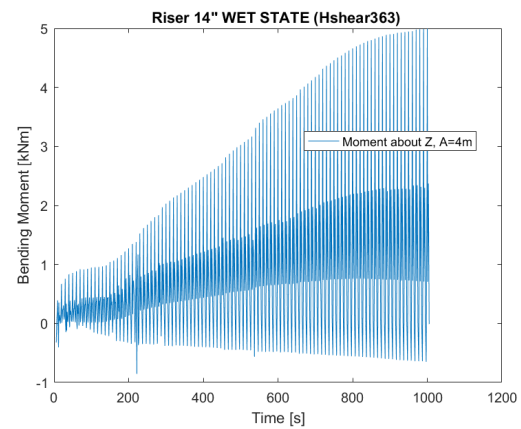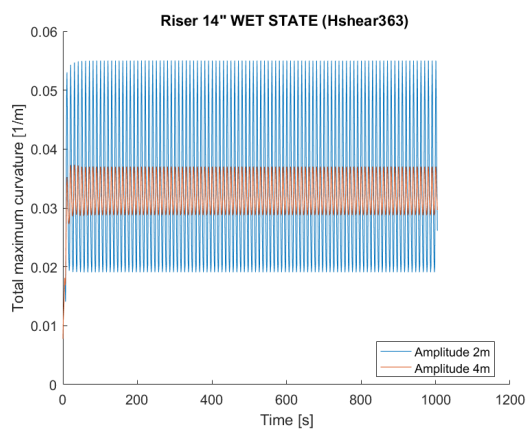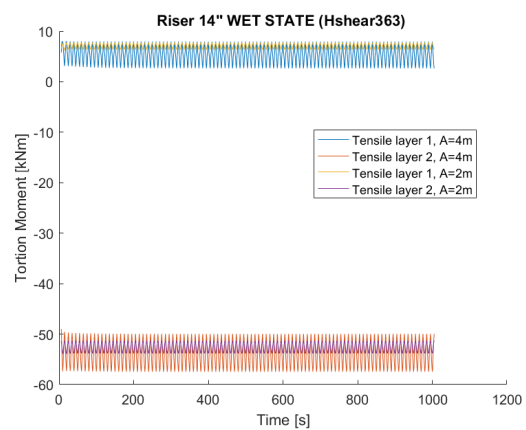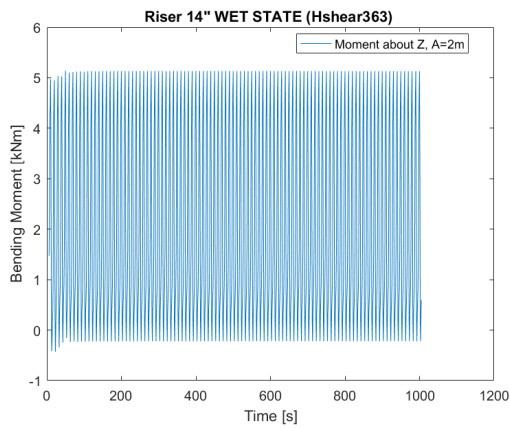
(c) Bending Moment About z, A=2m
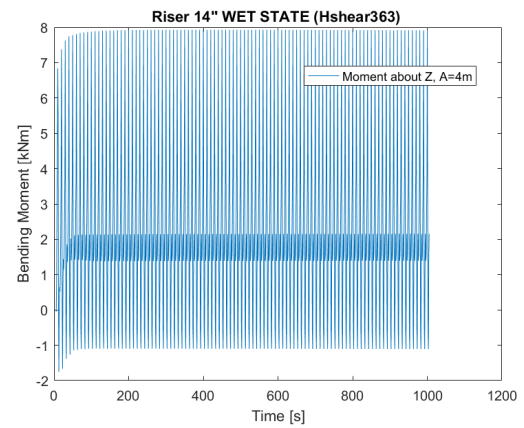
(d) Bending Moment About z, A=4m

Figure 8.12: Riser14", h=370m: Bending Moment at TDZ vs. Time.

Chapter 9

Local Effects and Built in Torque

9.1   Method Local Effects and Built in Torque

As there were no kink formations in the results from Chapter 8, it was decided to do a new set of analysis in order try to test the limits. The calculations were mostly preformed the same way as in Chapter 8. However, in this case the water depth has been increased to beyond critical level, resulting in a depth of 480m for the 6" pipe and 420m for the 14" pipe.

In addition, a prescribed torsion of the top end with value π, was added over a time $t = 10$s before the oscillations. This resulted in a total time of 1015s for the whole analysis.

9.2   Result Local Effects and Built in Torque

First comparing the new curvature results with those of Chapter 8, the maximum total curvatures of the 6" pipe is about the same in both cases (see Figure 8.4a & 9.2a), while it has been reduced for the case of the 14" pipe (see Figure 8.7a & 9.5a). Consequently, there are no kink formations.

When it comes to torque, there is, compared to the previous analysis, an increase in the absolute value of the outer tensile layer (see Figure 8.4b, 8.7b, 9.2b & 9.5b). The inner tensile layer on the other hand, has in general the same value as before. This shows that there is an increase in the torsion instability with increase of water depth together with addition of torque. The increased imbalance between the tensile armour layers is also evident in the axial wire stress (see Figure 8.5, 8.8 9.3 & 9.6).

In contrast to the solutions of the analysis in Chapter 8, all solutions in this case appears to be stable. This indicates that the solution can be trusted, and that there will be no kink formations at this water level.
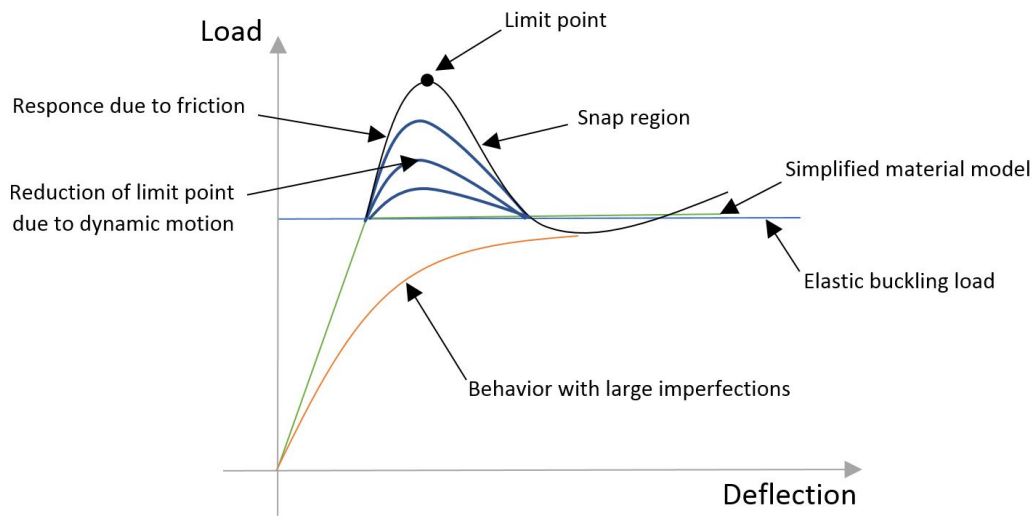
Figure 9.1: Buckling and Post-Buckling Model

The buckling model for local lateral buckling of the inner tensile armour used in the analysis in Chapter 8 & 9, is a simplified model as seen in Figure 9.1. The model assumes that buckling will occur in the inner tensile layer, at the value of the elastic buckling load found from Equation 1.38. Focusing on the post-buckling behaviour, the inner layer looses its ability to carry any further load and the axial stiffness becomes next to zero. Consequently the outer tensile layer is forced to carry the excessive load, creating torsion imbalance.

In reality, due to friction, the buckling limit is much higher than the elastic buckling load, it is normal to talk about the limit point. If the limit point is exceeded, the structure will quickly lose its capacity, in something that is described as the snap region. This region is hard to capture in calculation, as it gives several possibilities of equilibrium at the same load.

The mechanics of buckling in real life is very complex, as friction may increase the structures buckling resistance, dynamic motion and imperfections will reduce the capacity. The method presented in this paper is an attempt to establish a way to determine the safety against torsion instability for design and planing purposes, in relation to other failure modes. This is to be done within reasonable computational power. The result from the analysis shows that for global torsion buckling to occur, the design limitations have to be well stretched. This is a practise that is not common on the Norwegian shelf for flexible pipes, but may be more applicable in other regions. An alternative to the method presented here, is to include the friction and snap effect. By doing this, one may create a "kick" to trigger the kink formation.

(a) Maximum Total Curvature vs. Time.   (b) Torsion Moment at TDZ vs. Time
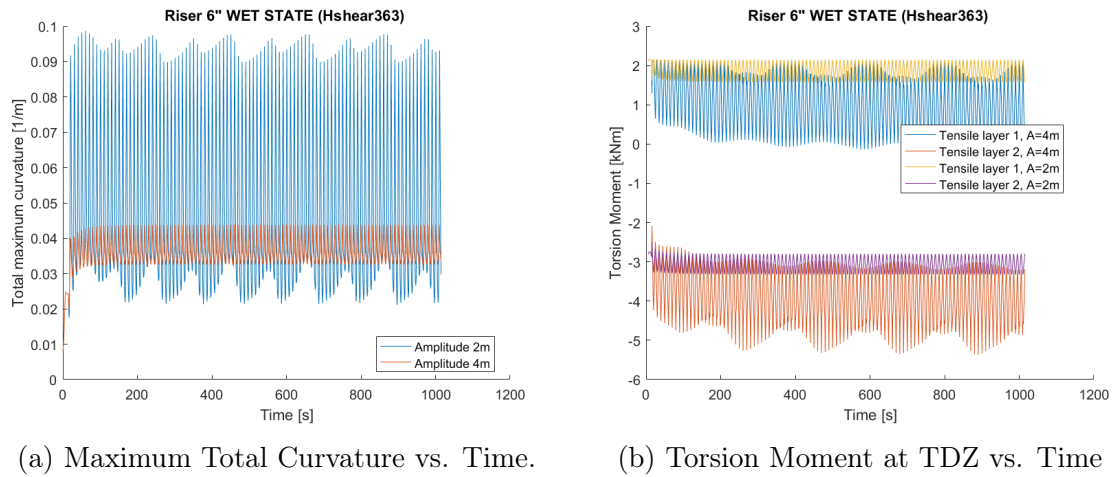
Figure 9.2: Riser 6", h=480: Curvature and Torsion Moment

(a) Amplitude 2m

(b) Amplitude 4m
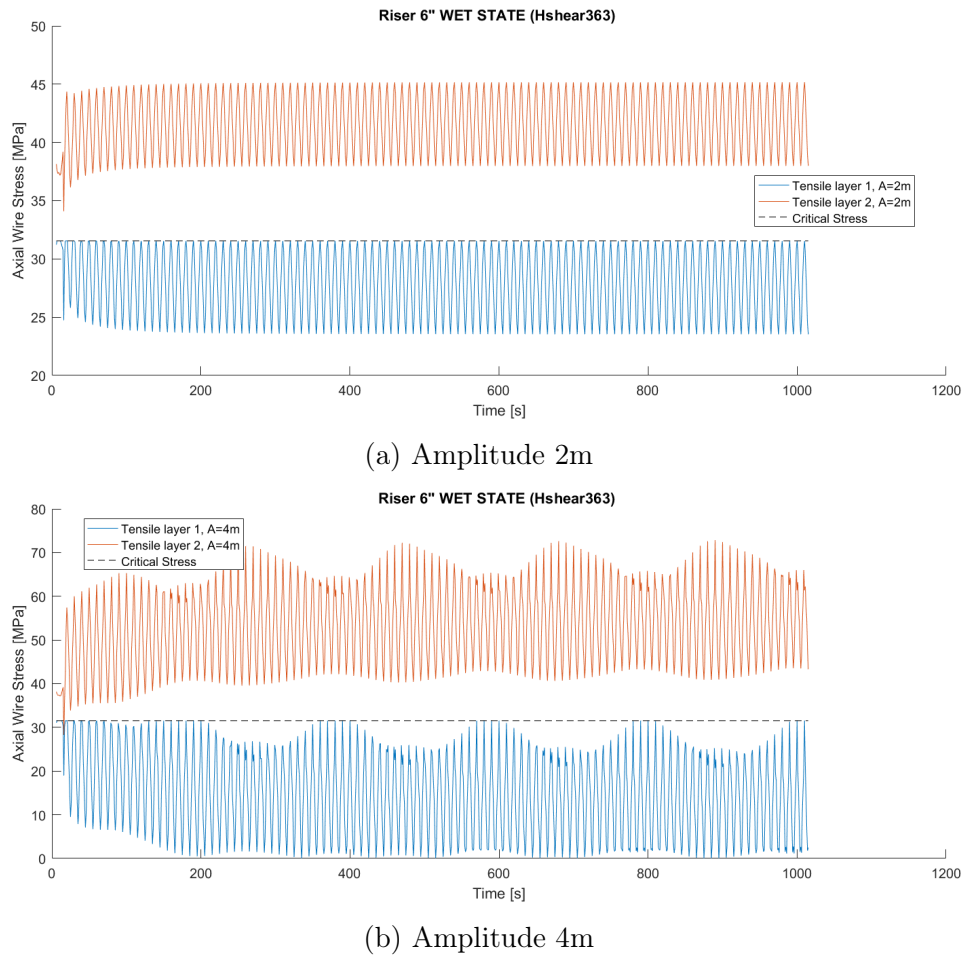
Figure 9.3: Riser 6", h=480: Axial Wire Stress at TDZ vs. Time.
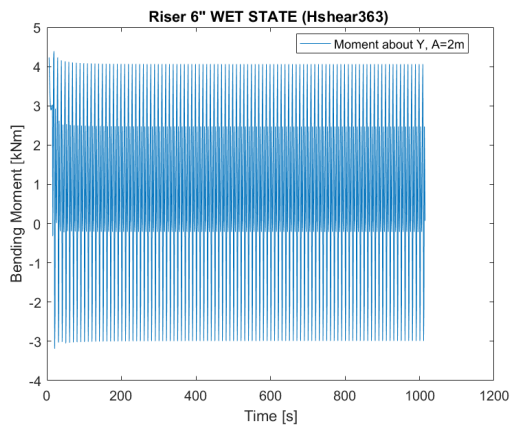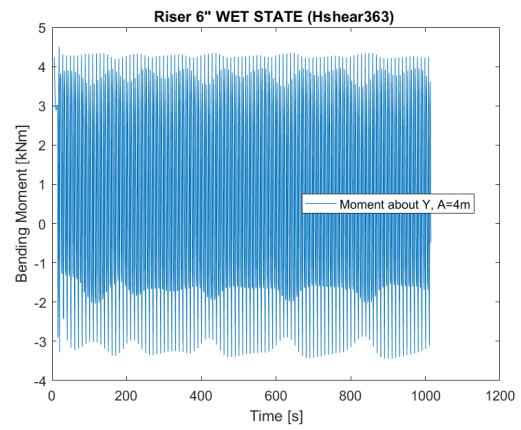
(a) Bending Moment About y, A=2m

(b) Bending Moment About y, A=4m
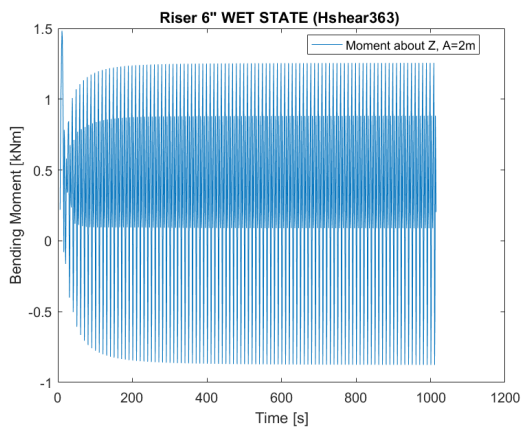
(c) Bending Moment About z, A=2m
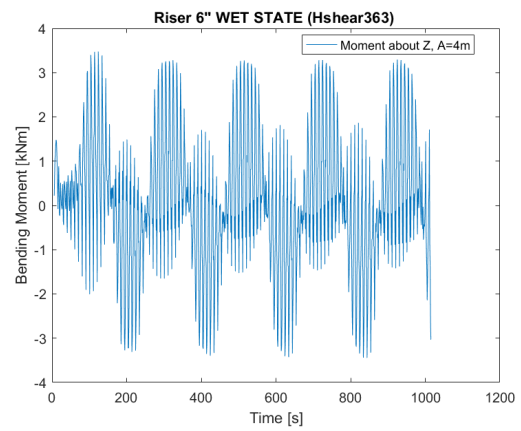
(d) Bending Moment About z, A=4m

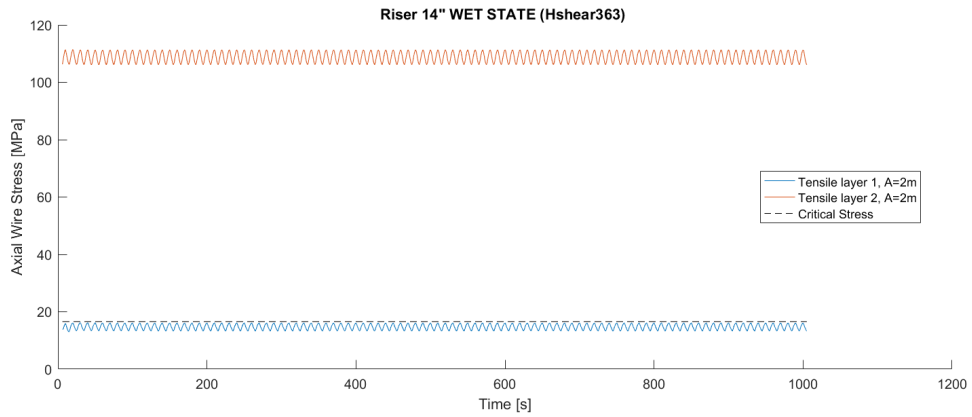Figure 9.4: Riser6", h=480: Bending Moment at TDZ vs. Time.
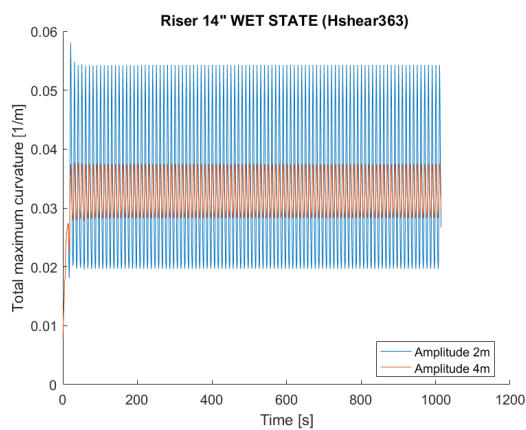

(a) Maximum Total Curvature vs. Time.
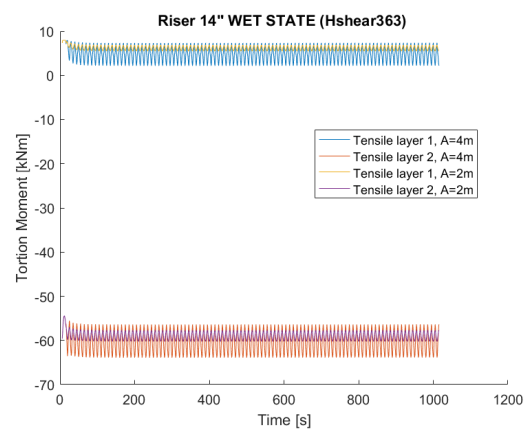
(b) Torsion Moment at TDZ vs. Time

Figure 9.5: Riser 14", h=420: Curvature and Torsion Moment
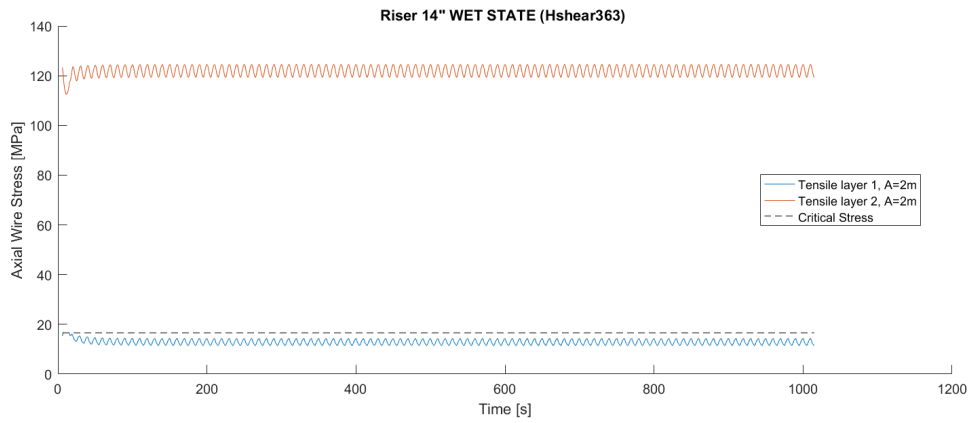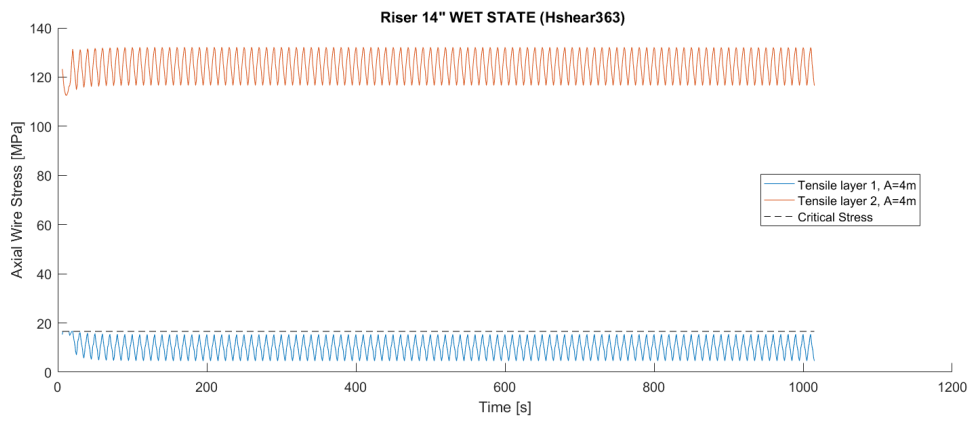
(a) Amplitude 2m

(b) Amplitude 4m

Figure 9.6: Riser 14", h=420: Axial Wire Stress at TDZ vs. Time.
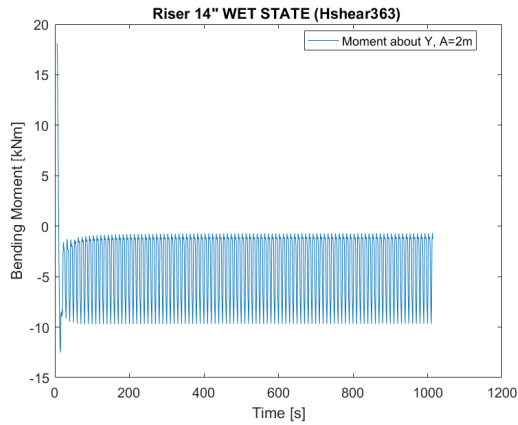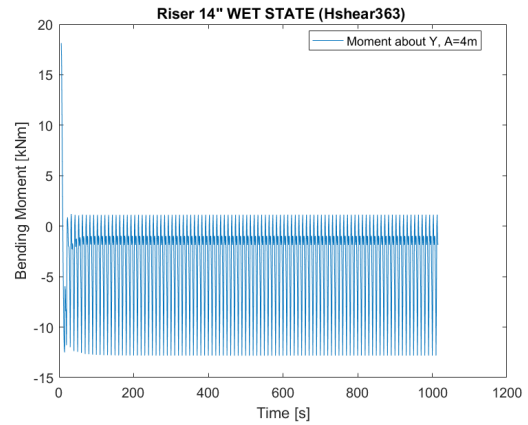
(a) Bending Moment About y, A=2m

(b) Bending Moment About y, A=4m
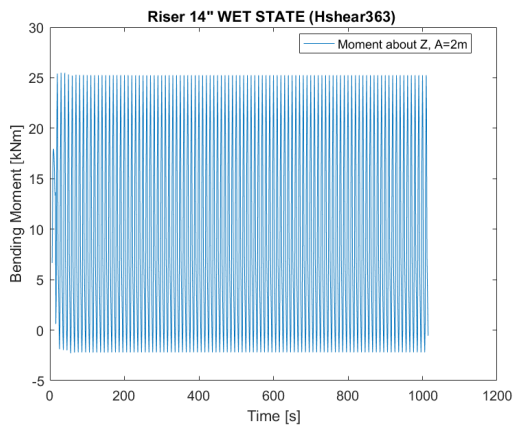
(c) Bending Moment About z, A=2m
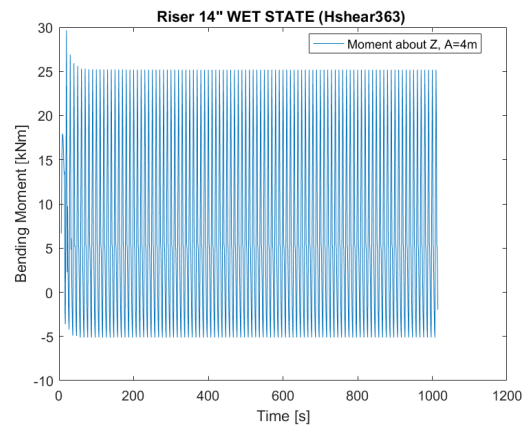
(d) Bending Moment About z, A=4m

Figure 9.7: Riser14", h=420: Bending Moment at TDZ vs. Time.

Chapter 10

Final Remarks

10.1 Conclusions

The purpose of this paper is to further the knowledge of torsion instability of flexible dynamic risers in catenary configuration, with particular weight on flexible pipes. It has been focused on critical installation and operating scenarios, in order to establish a methodology that is useful in planing and design processes.

Before the main analysis, a prestudy was done in order to determine the global stiffness quantities. The results from the Bflex2010 calculations, showed that the values of axial stiffness and torsion stiffness, were in general the same for equal geometries, independent of the state of the annulus (flooded/dry). In addition, the calculated initial bending stiffness also displayed independence of state, while slip moment and curvature along with post-slip stiffness showed great dependence on state. These results are in line with established theory, and where therefore deemed sufficiently accurate.

In the case of flooded annulus, the bending stiffness was significantly lower than for the same geometry in dry state. This is due to the reduction in friction between the layers, and makes the wet state the most critical. As tear and leakage in the outer-sheet is fairly common, it is recommended that this failure mode is accounted for in design calculations.

Looking back at the elastic case analyses, preformed by using the Pipe31 element, an initial analytic approximation was preformed to predict the critical torque using the Greenhill formula. Even though previous studies suggests that this is a good approximation method for risers in catenary configuration, the results showed that the analytic formula severely underestimated the pipe strength in the case of dry annulus.

However, unlike previous works, the analysis in this case considered geometries with larger cross-section diameter, resulting in high bending stiffness. Additionally, it was

assumed that both ends of the riser were fixed against translation, which is in conflict with the established assumptions of the Greenhill formula. The resulting conclusion is that the Greenhill formula is still a usable method for initial prediction, in lack of a better alternative.

The choice between assuming that both ends are fixed against translation, or letting the tail end resting on the seabed to be only restricted by friction, should be seriously considered in relation to the specific real case. For general analysis it is recommended to have translation only being restrained by friction at the tail end, as it is the most critical condition.

Setting the elastic case model (Pipe31) in comparison with the non-linear model (Compipe42), it becomes evident that the elastic model is not always suitable to best describe the critical curvature and torque for flexible pipes. A way to test the suitability of the elastic model before analysis, is to compare the slip curvature to the maximum allowable design curvature. If the slip curvature is higher, one can conclude that buckling will either happen in the elastic region, or beyond already established design limits. In the case of flooded annulus, the slip curvature is relatively low. Thus, non-linear analysis taking into consideration the effect of slip, is recommended in wet case.

For the initial dynamic heave scenarios with built in torque, not taking into account local effects, the analysis shows that exceeding the critical curvature is a clear indication of kink formation. On the other hand, it becomes evident that the established critical torsion from the previous analysis is too great. This leads to the conclusion that the prediction of critical torsion is highly dependant on the length of the application time for the prescribed rotation.

Considering the extended heave scenario, one sees that the increase in curvature, due to the heave motion, is decreasing, and will converge towards zero. However, note that the increase in curvature does not necessarily propagate faster for higher waves. Instead, for certain circumstances the opposite is the case. This is assumed to be happening because the higher waves are able to completely stretch out the pipe again after the wave trough. As a consequence of this, several wave amplitudes must be tested in order to get a reliable result.

Finally, focusing on the coupling model between global and local effects, there are no kink formations. Also, all the analysis of the pipes at critical or deeper water depths, are stable. From this follows that the methodology is useful and the solution may be trusted. In this case, resulting in deeming the water depth acceptable. On the other hand, the model with under critical water depth has an unstable solution, were natural resistance is built up instead. The final conclusion is that in order for global torsion buckling to occur, the design limits have to be gravely pushed or even overstepped.

10.2   Recommendations for Further Work

For further work on the topic of global torsion instability, it is recommended to conduct scale laboratory experiments with the purpose to reproduce the elastic and non-linear riser scenarios described in the thesis. Based on the experimental results, a verdict about the numerical accuracy of BFLEX2010 can be derived.

In the thesis, different dynamic analysis of cyclic heave motion have been performed, both for elastic and non-linear models. However, typically the motion of the installation vessel is much more complex compared to pure heave motion. Therefore, it is proposed to expand the complexity of the imposed motion on the riser, also taking into consideration sway, surge, roll components, etc.

It would also be interesting to dive further into the connection between local and global effects. In this paper, only transverse lateral buckling has been accounted for, while the effects of of birdcaging and collapse of the carcass, have not been explored.

Another interesting field is the different riser configurations. This paper focuses on the catenary configuration in relation to the J-installation method. However, other configurations may give a different view on the torsion instability problem. So far the presented methodologies in the literature on global torsion, only considers the catenary configuration, and there are no established methods for the other cases.

Bibliography

API17J (2014), 4 edn, American Petrolium Institute.

Bažant, Z. P. & Cedolin, L. (1991), *Stability of structures : elastic, inelastic, fracture, and damage theories*, Vol. 26 of *The Oxford engineering science series*, Oxford University Press, New York, chapter 1, pp. 1–49.

Irgens, F. (2014), *Formulars mechanics*, 2 edn, Fagbokforlaget.

Koloshkin, E. (2016), Torsion buceling of dynamik flexible risers, Master's thesis, The Norvegian University of Sience and Technology (NTNU).

MARINTEK BEFLEX Dev. Team (2016), *BFLEX 2010 User Manual*, 3 edn, MAR-INTEK.

Moan, T. (2003), *TMR 4190 Finite Element Modelling and Analysis of Marine Structures*, akademika" forlag, Marine Technonogy Centre, Trondheim, Norway.

Neto, A. G. & de Arruda Martins, C. (2013), 'Structural stability of flexible lines in catenary configuration under torsion', *Marine Structures* **34**, 16 – 40.
URL: *http://www.sciencedirect.com/science/article/pii/S0951833913000518*

Rabelo, M., Pesce, C., Santos, C., Ramos, R., Franzini, G. & Gay Neto, A. (2015), 'An investigation on flexible pipes birdcaging triggering', *Marine Structures* **40**, 159–182. cited By 1.
URL: *https://www.scopus.com/inward/record.uri?eid=2-s2.0-84913572936&partnerID=40&md5=446a825699ce45bfd915aec4077de0ff*

Sævik, S. (2011), 'Theoretical and experimental studies of stresses in flexible pipes', *Computers and Structures* **89**(23-24), 2273–2291. cited By 42.
URL: *https://www.scopus.com/inward/record.uri?eid=2-s2.0-800550026211&partnerID=40&md5=1f548d4d16a0067a6a0f05c03197df0f*

Sævik, S. (2013), BFLEX2010 - teory manual, Marintek report, Norwegian Marine Technology Research Institute, Marine Technonogy Centre, Otto Nilsens Veg 10, Trondheim, Norway.

Sævik, S. (2015), Lecture notes in offshore pipeline technology. Originaly written spring 2011 to support lectures given in Pipline Technology at Department of Marine Technology, NTNU.

Sævik, S. & Ji, G. (2014), Differential equation for evaluating transverse buckling behavior of tensile armour wires, *in* 'ASME 2014 33rd International Conference on Ocean, Offshore and Arctic Engineering', American Society of Mechanical Engineers, pp. V06BT04A021–V06BT04A021.

Sævik, S. & Koloshkin, E. (2017), Torsion instability of offshore cables during installation, *in* 'To be published: ASME 2017 36st International Conference on Ocean, Offshore and Arctic Engineering', American Society of Mechanical Engineers.

Sævik, S. & Thorsen, M. J. (2012), Techniques for predicting tensile armour buckling and fatigue in deep water flexible pipes, *in* 'ASME 2012 31st International Conference on Ocean, Offshore and Arctic Engineering', American Society of Mechanical Engineers, pp. 469–482.

Vaz, M. & Rizzo, N. (2011), 'A finite element model for flexible pipe armor wire instability', *Marine Structures* **24**(3), 275–291. cited By 23.
URL: *https://www.scopus.com/inward/record.uri?eid=2-s2.0-79958036377&partnerID=40&md5=758fcee2dd821054a63b8e71d6f2d144*

Appendix A

Computer Input Files

A.1   Bflex2010: Elastic case, wet state, step 1

```
HEAD PIPE31 MODEL
HEAD 6" PIPE: WET STATE

#_____
#
#CONTROL DATA:
#        MAXIT    NDIM    ISOLVR  NPOINT  IPRINT  CONVR   GAC      ISTRES
CONTROL 100      3        2       16      01      1E-6    9.81     STRESSFREE

#Dynamic Analysis criteria:
#        MSTAT    ALPHA1  ALPHA2  ALPHA
DYNCONT 1        0.0      0.051   -0.05

#ANALYSIS TIME CONTROL:
#      T   DT DTVI    DT0     TYPE    STEPTYPE    ITERCO  ITCRIT  MAXIT   MAXDIV  CONR
TIMECO 5.0 0.1 1.0   201.0   STATIC  AUTO        NONE    ALL     300     5       1E-5

#RESULT VISUAL DEFENITION:
#        MODE        FACTOR  RESULT
VISRES integration  1       sigma-xx

#_____
# GEOMETRY

#PIPE
#        TYBE         NID       X      Y    Z
NOCOOR COORDINATES    1         0      0    -1999.894953
REPEAT 540 1 1 0 0
NOCOOR COORDINATES    541       539.2  0    -1999.894953
REPEAT 770 1 0.2 0 0
NOCOOR COORDINATES    1311      695    0    -1999.894953
REPEAT 988 1 2 0 0


#ELCON DATA for PIPE
#        ELGR      ELTY       CROSSNAME   ELID    NOD1    NOD2
ELCON    PIPE1     PIPE31     PIPEMAT1    1       1       2
REPEAT 539 1 1
ELCON    PIPE2     PIPE31     PIPEMAT1    540     540     541
REPEAT 770 1 1
ELCON    PIPE3     PIPE31     PIPEMAT1    1310    1310    1311
REPEAT 988 1 1

#SEABED
#        NAME    TYPE    SURFACEID    EID      NID
ELCON    SEABED CONT126  COSURF1      10001     1
REPEAT 2298 1 1

#SEASURFACE NODE
#        TYPE         NID       X     Y      Z
NOCOOR COORDINATES    20001     0    -200    0
                      20100     2670 -200    0
REPEAT 3 100 0 200.0 0
#        NAME    TYPE    MID      EID         NID
ELCON    SEA1    SEA150  SEAMAT   20001       20001 20002 20102 20101
REPEAT 99 1 1
REPEAT 2 99 100


#_____
#ORIENT INPUT

#PIPE
#                        ELNO        X         Y         Z
ELORIENT COORDINATES     1           0.0       1.000     -1999.894953
REPEAT 2297 1 0 0 0
#SEABED                  ELNO        TX        TY        TZ
ELORIENT EULERANGLE      10001       0.000     0.000     0.0
REPEAT 2298 1 0 0 0


#_____

#ELEMENT DATA(PIPE DATA)
#    NAME  TYPE RAD      TH      RCD TCD RMADD TMADD MD    MS       ODP   ODW   RKS PHIST
ELPROP PIPE1 PIPE 0.09385 0.0353 1.0 0.1 2     1.0   8.16E1 4.276E1 0.223 0.223 0.5 100
ELPROP PIPE2 PIPE 0.09385 0.0353 1.0 0.1 2     1.0   8.16E1 4.276E1 0.223 0.223 0.5 100
ELPROP PIPE3 PIPE 0.09385 0.0353 1.0 0.1 2     1.0   8.16E1 4.276E1 0.223 0.223 0.5 100
```

```
#_____
# BONDRARY CONDITION
#PIPE
#         COSYS     NODEID    DOF
BONCON  GLOBAL      1        2
BONCON  GLOBAL      1        3
BONCON  GLOBAL      1        4
BONCON  GLOBAL      1        6

BONCON  GLOBAL      2298     1
BONCON  GLOBAL      2298     2
BONCON  GLOBAL      2298     4
BONCON  GLOBAL      2298     6

#SEA
BONCON   GLOBAL   20001       1
REPEAT 300 1
BONCON   GLOBAL   20001       2
REPEAT 300 1
BONCON   GLOBAL   20001       3
REPEAT 300 1

#SEABED DATA/CONTACT ELEMENT
#           NAME    COFILE                  NLIN   KP0    XS      YS  ANGSTART    MLINEID
COSURFPR    COSURF1 "seabed_2000_flat.txt"  3      0.0    0.0    0.0  0.0         100 101
102
#         ROUTE ID        KP1          KP2    SOILTYPE
COSUPR       100          0.0     100000.0    soil1
COSUPR       101          0.0     100000.0    soil1
COSUPR       102          0.0     100000.0    soil1

#CONTACT INTERFACE DATA
#        GROUPN     MNAME          NAME    IS1    ISN   ISTX   ISTY  ISTZ   MAXIT  IGAP
CONTINT SEABED      PIPE1          COSURF1  1     540    5.0    5.0   0.0    60     2
CONTINT SEA1        SEA1           PIPE1

CONTINT SEABED      PIPE2          COSURF1  541   1310   5.0    5.0   0.0    60     2
CONTINT SEA1        SEA1           PIPE2

CONTINT SEABED      PIPE3          COSURF1  1311  2298   5.0    5.0   0.0    60     2
CONTINT SEA1        SEA1           PIPE3

#_____

#LOAD INPUT
#External Pressure and Gravity Load
#        PRESHIST GRAVHIST
PELOAD 100          100
#     HIST DIR NODE LOAD
CLOAD 150   1    1  -1E3
#       seagrp type    wavno hist    x0  y0 phi  T     H   D       Phase
WAVELO SEA1   REGULAR 100   100   -1000 0  0.000 10.0 0.0 2000   0

# LIFTING END OF PIPE TO SEA SURFACE
#PRESCRIBED DISPLACEMENT
#           PDTYPE NODID DOF DISPVAL HISTNO
CONSTR PDISP GLOBAL 2298   3  2000.0  300

# HISTORY
THIST 100   0.0    0.0
            0.1    1.0
            1.0    1.0

THIST 150   0.0    50.0
            4.8    50.0
            5.0    1.0

THIST 300   0.0    0.0
            4.8    1.0

THIST_r 400 5.0 45.0 rampcos 1.0

#_____
# MATERIAL DATA
# PIPE:
#       name      type   poiss talf tec hc beta ea    eiy    eiz    git    em    gm
```

```
MATERIAL pipemat1 linear 0.2   0    0   0  0     6.33E8 1.99e4 1.99e4 1.59e6 2.1e11 8.1e10

#SEA
MATERIAL SEAMAT SEA 1.024E3

#SEABED
#          name      type       MUX     MUY  XNAME   YNAME    ZNAME
MATERIAL  soil1     CONTACT    0.4     1.0  soilx   soily    soilz
#          name      type     IHARD  EPS        SIGMA
MATERIAL  soilx     epcurve  1      0.00       0.0
                                    0.005      1.0
                                    2.00       1.01

MATERIAL  soily     epcurve  1      0.00       0.0
                                    0.02       1.0
                                    2.00       1.01

MATERIAL  soilz     hycurve       -2000.0     -130E6
                                   2000.0      130E6
```

A.2 Bflex2010: Elastic case, wet state, step 2

```
HEAD PIPE31 MODEL
HEAD 6" PIPE: WET STATE

#_____
#
#CONTROL DATA:
#       MAXIT    NDIM    ISOLVR  NPOINT  IPRINT  CONVR   GAC     ISTRES
CONTROL 100      3       2       16      01      1E-6    9.81    RESTART 50

#Dynamic Analysis criteria:
#       MSTAT    ALPHA1  ALPHA2  ALPHA
DYNCONT 1        0.0     0.051   -0.05

#ANALYSIS TIME CONTROL:
#       T        DT      DTVI    DT0     TYPE    STEPTYPE  ITERCO  ITCRIT  MAXIT  MAXDIV  CONR
TIMECO  5.0      0.1     1.0     201.0   STATIC  AUTO      NONE    ALL     300    5       1E-5
TIMECO  30.0     0.01    2.0     201.0   dynamic AUTO      none    ALL     20     5       1e-5
TIMECO  45.0     0.01    0.5     201.0   dynamic AUTO      none    ALL     20     5       1e-5

#RESULT VISUAL DEFENITION:
#       MODE            FACTOR  RESULT
VISRES  integration  1          Vcondis-y vcondis-z vconfor-y sigma-xx vconfor-z

#_____
# GEOMETRY

#PIPE
#       TYBE            NID     X       Y       Z
NOCOOR  COORDINATES     1       0       0       -1999.894953
REPEAT 540 1 1 0 0
NOCOOR  COORDINATES     541     539.2   0       -1999.894953
REPEAT 770 1 0.2 0 0
NOCOOR  COORDINATES     1311    695     0       -1999.894953
REPEAT 988 1 2 0 0


#ELCON DATA for PIPE
#       ELGR     ELTY           CROSSNAME   ELID    NOD1    NOD2
ELCON   PIPE1    PIPE31         PIPEMAT1    1       1       2
REPEAT 539 1 1
ELCON   PIPE2    PIPE31         PIPEMAT1    540     540     541
REPEAT 770 1 1
ELCON   PIPE3    PIPE31         PIPEMAT1    1310    1310    1311
REPEAT 988 1 1

#SEABED
#       NAME     TYPE    SURFACEID   EID     NID
ELCON   SEABED CONT126   COSURF1     10001     1
REPEAT 2298 1 1

#SEASURFACE NODE
#       TYPE            NID     X       Y       Z
NOCOOR  COORDINATES     20001     0     -200     0
                        20100   2680    -200     0
REPEAT 3 100 0 200.0 0
#       NAME    TYPE    MID     EID          NID
ELCON   SEA1    SEA150  SEAMAT  20001      20001 20002 20102 20101
REPEAT 99 1 1
REPEAT 2 99 100

#_____
#ORIENT INPUT

#PIPE
#                       ELNO            X           Y           Z
ELORIENT COORDINATES    1               0.0     1.000       -1999.894953
REPEAT 2297 1 0 0 0
#SEABED                 ELNO            TX      TY      TZ
ELORIENT EULERANGLE     10001           0.000   0.000       0.0
REPEAT 2298 1 0 0 0

#_____

#ELEMENT DATA(PIPE DATA)
#       NAME  TYPE RAD      TH     RCD TCD RMADD TMADD MD    MS       ODP   ODW   RKS PHIST
ELPROP PIPE1 PIPE 0.09385 0.0353 1.0 0.1 2     1.0   8.16E1 4.276E1 0.223 0.223 0.5 100
ELPROP PIPE2 PIPE 0.09385 0.0353 1.0 0.1 2     1.0   8.16E1 4.276E1 0.223 0.223 0.5 100
ELPROP PIPE3 PIPE 0.09385 0.0353 1.0 0.1 2     1.0   8.16E1 4.276E1 0.223 0.223 0.5 100

#_____
```

```
# BONDRARY CONDITION
#PIPE
#         COSYS     NODEID    DOF
BONCON  GLOBAL      1         1
BONCON  GLOBAL      1         2
BONCON  GLOBAL      1         3
BONCON  GLOBAL      1         4
BONCON  GLOBAL      1         6

BONCON  GLOBAL      2298      1
BONCON  GLOBAL      2298      2
BONCON  GLOBAL      2298      3
BONCON  GLOBAL      2298      4
BONCON  GLOBAL      2298      5


#SEA
BONCON   GLOBAL   20001        1
REPEAT 300 1
BONCON   GLOBAL   20001        2
REPEAT 300 1
BONCON   GLOBAL   20001        3
REPEAT 300 1

#SEABED DATA/CONTACT ELEMENT
#          NAME    COFILE                NLIN   KP0    XS      YS ANGSTART    MLINEID
COSURFPR    COSURF1 "seabed_2000_flat.txt" 3     0.0    0.0    0.0   0.0         100 101 102
#       ROUTE ID          KP1         KP2    SOILTYPE
COSUPR      100          0.0      100000.0   soil1
COSUPR      101          0.0      100000.0   soil1
COSUPR      102          0.0      100000.0   soil1


#CONTACT INTERFACE DATA
#       GROUPN     MNAME         NAME    IS1    ISN    ISTX    ISTY   ISTZ   MAXIT  IGAP
CONTINT SEABED      PIPE1        COSURF1  1      540    5.0     5.0    0.0    60     2
CONTINT SEA1        SEA1         PIPE1

CONTINT SEABED      PIPE2        COSURF1  541    1310   5.0     5.0    0.0    60     2
CONTINT SEA1        SEA1         PIPE2

CONTINT SEABED      PIPE3        COSURF1  1311   2298   5.0     5.0    0.0    60     2
CONTINT SEA1        SEA1         PIPE3

#_____

#LOAD INPUT
#External Pressure and Gravity Load
#        PRESHIST GRAVHIST
PELOAD  100          100
#     HIST DIR NODE LOAD
CLOAD 150   1    1  -1E3
#     seagrp type    wavno hist    x0  y0 phi  T    H   D      Phase
WAVELO SEA1   REGULAR 100   100    -1000 0 0.000 10.0 0.0 2000   0

#PRESCRIBED DISPLACEMENT
#          PDTYPE NODID DOF DISPVAL HISTNO
CONSTR PDISP GLOBAL 2298   6   90      400

# HISTORY
THIST 100    0.0     0.0
             0.1     1.0
             1.0     1.0

THIST 150    0.0     50.0
             4.8     50.0
             5.0     1.0

THIST 300    0.0     0.0
             4.8     1.0


THIST_r 400 5.0 45.0 rampcos 1.0


#_____
# MATERIAL DATA
# PIPE:
#        name     type   poiss talfa tecond heatc beta ea      eiy      eiz      git     em     gm
MATERIAL pipemat1 linear 0.2   0     0      0     0    6.33E8 1.99e4 1.99e4 1.59e6 2.1e11 8.1e10

#SEA
MATERIAL SEAMAT SEA 1.024E3
```

```
#SEABED
#          name      type     MUX     MUY  XNAME   YNAME   ZNAME
MATERIAL  soil1    CONTACT   0.4     1.0  soilx   soily   soilz
#          name      type    IHARD  EPS       SIGMA
MATERIAL  soilx    epcurve  1      0.00      0.0
                                   0.005     1.0
                                   2.00      1.01

MATERIAL  soily    epcurve  1      0.00      0.0
                                   0.02      1.0
                                   2.00      1.01

MATERIAL  soilz    hycurve        -2000.0   -130E6
                                   2000.0    130E6
```

```
#          name      type     MUX     MUY  XNAME   YNAME   ZNAME
MATERIAL  soil1    CONTACT   0.4     1.0  soilx   soily   soilz
```

A.3 Bflex2010post: Elastic case, wet state

```
# Element moment history plot
#Core
#        RAFPRE       MPFPRE  XLEG
ELPLOT "Riser6pipe31_2" "Riser6M" "'Rotation dof 6 global (rad)'"
# XRES    YLEG                     XRES     EL1 EL2 XSCL YSCL END
 HIST400 "'Moment about X (kNm)'"  ELMOM-X 2296 2296 90  1e-3 2


# Element force history plot

#        RAFPRE       MPFPRE  XLEG
ELPLOT "Riser6pipe31_2" "Riser6G" "'Time (s)'"
# XRES    YLEG                 XRES         EL1 EL2 XSCL  YSCL END
 TIME "'Tention in x (kN)'" ELFORCE-X   1309 1309 1     1e-3 2


#Global ELement PLOTs

#        RAFPRE              MPFPRE
GLPLOT  "Riser6pipe31_2"    "6GLPLOTs_y"
# XLEG                         XRES    YLEG                          YRES
  "Length along riser (m)"  E-COR   "Curvature about y (1/m)"   ELCUR-Y
# FELID LELID   XSCL     YSCL     ELEND
  1     2297    1        1        2



#        RAFPRE              MPFPRE
GLPLOT  "Riser6pipe31_2"    "6GLPLOTs_z"
# XLEG                         XRES    YLEG                          YRES
  "Length along riser (m)"  E-COR   "Curvature about z (1/m)"   ELCUR-Z
# FELID LELID   XSCL     YSCL     ELEND
  1     2297    1        1        2
```

A.4 Matlab: Elastic case, wet state

```matlab
fileID=fopen('Riser6M.mpf','r');
for i=1:13
fgets(fileID);
end
M=fscanf(fileID,'%e',[2,inf])';
fclose(fileID);

fileID=fopen('Riser6G.mpf','r');
for i=1:13
fgets(fileID);
end
g=fscanf(fileID,'%e',[2,inf])';
fclose(fileID);

[gmax,idx]=max(g(:,2));
l=2500;
EI=1.99e4;
G=2*sqrt(EI*gmax*1e3+(EI*pi/l)^2)*1e-3;
G2=2*sqrt(EI*1e3+(EI*pi/l)^2)*1e-3;
figure
hold on
plot(M(:,1),M(:,2));
plot([M(1,1),M(end,1)],[G,G],'--');
plot([M(1,1),M(end,1)],[G2,G2],'--');
title('Riser 6" WET STATE (Pipe31)')
xlabel('Impost rotation [rad]')
ylabel('Moment about X [kNm]')
legend('BFLEX2010',['Greenhill T=',num2str(g(idx,2)),'kN'],'Greenhill T_0', 'Location', 'northwest')
hold off

figure
plot(g(:,1),g(:,2));
title('Riser 6" WET STATE (Pipe31)')
xlabel('Time [s]')
ylabel('Element tension [kNm]')

[Y,~]=ReadGL(2297,45,'6GLPLOTs_y.mpf');
[Z,t]=ReadGL(2297,45,'6GLPLOTs_z.mpf');

%Calculating total curvature
S=zeros(size(Y));
S(:,1)=Y(:,1);
for i=1:length(t)
    S(:,i+1)=sqrt(Z(:,i+1).^2+Y(:,i+1).^2);
end

[v,idx2]=max(M(:,2));
tc=idx2+5;
Beta=5.13e-3;
K=1/1.6995;
figure
hold on
plot(S(:,1)',S(:,tc+1)','-','DisplayName','Curvature at buckling')
plot([S(1,1),S(end,1)],[Beta,Beta],'--','DisplayName','Slip Curvature')
plot([S(1,1),S(end,1)],[K,K],'--','DisplayName','Max Allowable Curvature')
hold off

title('Riser 6" WET STATE (Pipe31)')
xlabel('Coordinat along riser [m]')
ylabel('Total curvature [1/m]')
legend('Location','northeast')
```